

## Research Article

# Heat Kernel of Networks with Long-Range Interactions

Franck Kalala Mutombo <sup>1,2</sup>, Alice Nyanzi,<sup>2,3</sup> and Simukai W. Utete<sup>2</sup>

<sup>1</sup>Department of Mathematics and Computer Sciences, University of Lubumbashi, Route Kasapa 1825, Democratic Republic of the Congo

<sup>2</sup>African Institute for Mathematical Sciences, AIMS-South Africa, 5-6 Melrose Road, Muizenberg 7945, South Africa

<sup>3</sup>Stellenbosch University, Stellenbosch 7600, South Africa

Correspondence should be addressed to Franck Kalala Mutombo; [franckm@aims.ac.za](mailto:franckm@aims.ac.za)

Received 27 December 2022; Revised 30 October 2023; Accepted 24 January 2024; Published 31 March 2024

Academic Editor: Hiroki Sayama

Copyright © 2024 Franck Kalala Mutombo et al. This is an open access article distributed under the Creative Commons Attribution License, which permits unrestricted use, distribution, and reproduction in any medium, provided the original work is properly cited.

The heat kernel associated with a discrete graph Laplacian is the basic solution to the heat diffusion equation of a strict graph or network. In addition, this kernel represents the heat transfer that occurs over time across the network edges. Its computation involves exponentiating the Laplacian eigensystem with respect to time. In this paper, we expand upon this concept by considering a novel network-theoretic approach developed in recent years, which involves defining the  $k$ -path Laplacian operator for networks. Prior studies have adopted the notion of integrating long-range interactions (LRI) in the transmission of “information” across the nodes and edges of the network. Various methods have been employed to consider long-range interactions. We explore here the incorporation of long-range interactions in network analysis through the use of Mellin and Laplace transforms applied to the  $k$ -path Laplacian matrix. The contribution of this paper is the computation of the heat kernel associated with the  $k$ -path Laplacian, called the generalized heat kernel (GHK), and its employment as the basis for extracting stable and useful novel versions of invariants for graph characterization. The results presented in this paper demonstrate that the use of LRI improves the results obtained with classical diffusion methods for networks characterization.

## 1. Introduction

A complex network can be conceptualized as a graph featuring a nontrivial topology comprising entities or components that serve as fundamental units within the system. This structure is complemented by a set of links or connections, delineating the relationships between these components. Networks are ubiquitous, spanning social, technological, ecological, and biological domains [1–3]. The importance of networks lies in their ability to represent complex systems, as these systems are commonly characterized by intricate interconnections [1, 4]. Graph objects can be seen as a radical reduction of complex systems. However, it has been shown that complex networks are very important tools for explaining many real complex systems in nature. To broaden the graph representation of complex systems, several researchers have introduced concepts beyond simple graphs. These include the use of hypergraphs

[5], multiplexes [6], and multilayer networks [6, 7]. In addition, there are temporal networks [8], and more recently,  $k$ -complexes and simplicial complexes [9–11]. However, these new representations do not generally consider the interactions/influences of nodes in the networks that are not directly connected such that the interaction decreases as the separation between nonconnected nodes increases. Dynamics on networks such as diffusion, consensus, and synchronization have recently attracted the attention of researchers. This is because of their applicability in various areas such as modeling of epidemic spread and diffusion of information in social networks, among others [12, 13]. It has been observed that in modeling of dynamic processes on networks that the substance in consideration, say information, heat, disease, rumor, and many more can propagate not only along direct edges of the network but also through indirect interactions. This approach has been successfully applied in [14, 15], and the authors explored

ways of accounting for these long-range interactions (LRI) using the social distance analogy which was associated with constraints in selection of the conductance parameter  $x$ . Recently, elegant approaches were put forward by Estrada [9, 16] that utilizes the Mellin and Laplace transforms of the graph Laplacian. Diffusion is, among others, the movement of substance such as heat or gas from a region of high concentration to a region of low concentration [4]. The modeling of diffusion processes on networks is a widely-used method to create simple models capturing the spread of phenomena like infections in a population, the dissemination of information in social networks (e.g., social network marketing), and the propagation of heat in conductors, among other applications [17]. Various diffusion-based models have been developed and discussed in the literature [13, 14, 18].

The heat diffusion process over an undirected graph/network having  $n$  nodes is given by

$$\frac{d\mathbf{u}}{dt} = -\mathbf{L}\mathbf{u}; \mathbf{u}(0) = \mathbf{u}_0, \quad (1)$$

where  $\mathbf{L} = \mathbf{D} - \mathbf{A}$  is the Laplacian matrix of the network with  $\mathbf{D}$  and  $\mathbf{A}$ , respectively, the degree and the adjacency matrices of the network. Let denote by  $\mathcal{L} = \mathbf{D}^{-1/2}\mathbf{L}\mathbf{D}^{-1/2}$  the normalized Laplacian matrix. The solution of equation (1) is given by

$$\mathbf{u}(t) = \mathbf{u}_0 \exp(-t\mathbf{L}). \quad (2)$$

In a state of equilibrium, the value of  $\mathbf{u}(t)$  converges uniformly across all nodes in the network. This converged value represents the average of the initial values assigned to all nodes and is given by

$$\alpha = \lim_{t \rightarrow +\infty} \mathbf{u}(t) = \frac{1}{n} \sum_{i=1}^n \mathbf{u}_i(0). \quad (3)$$

This happens as neighboring nodes in the network exchange heat until it is uniformly distributed across all interconnected nodes.

The heat kernel of equation (1) and given by

$$\mathbf{H}(t) = \exp(-t\mathbf{L}). \quad (4)$$

Expression (4) has been used as a means of network characterization and for graph clustering and amongst other applications [19]. Traditionally, the heat kernel, employed in these contexts, focuses on diffusion along the edges of the network, depicting the heat flow exclusively along these connections. In this work, however, we explore the heat kernel for which diffusion occurs at both short-range, that is, over the edges, and long-range, through nonadjacent nodes. Various models capturing these interactions have been proposed in the literature, including Random Walks with Levy Flights (RWLF) [20], the Fractional Diffusion Equation (FDE), and more recently, the  $k$ -path Laplacian-based model [9], among others. Over recent years, the heat kernel has found applications in diverse fields [21–25]. We embrace the model based on  $k$ -path Laplacian matrices as introduced by Estrada et al. [15]. The principal objective of this paper is to

formulate the heat kernel while considering long-range interactions. This involves extending the heat kernel (4) to accommodate long-range interactions when utilizing  $k$ -path Laplacian matrices in the exponentiation. The novel invariant derived from this extension is then applied for graph characterization. We conduct numerical experiments on both simple and random graphs to evaluate the impact of long-range interactions on the generalized heat kernel. Furthermore, we develop invariants associated with the generalized heat kernel and apply them for graph characterization. We explore two approaches for addressing long-range interactions: the Laplace transform and Mellin transform-based approaches presented in [15].

The structure of the paper is as follows: Section 2 provides an in-depth review of the  $k$ -path Laplacian concept. In Section 3, we introduce the generalized heat kernel (GHK). Section 4 follows the approach outlined in [19] to extract key invariants from the generalized heat kernel for graph characterization. These invariants include the trace, the zeta function, and the derivative at the origin of the generalized heat kernel. Section 5 delves into the generalized heat content, while Section 6 addresses the computational challenges associated with calculating the generalized heat kernel for large networks. The paper concludes with a discussion of findings and potential avenues for future research in the final section.

## 2. $k$ -Path Laplacian Matrices, $\mathbf{L}_k$

Let us consider an undirected graph  $G = (V, E)$  with finite or infinite vertices  $V$  and edges  $E$ . We assume that  $G$  is connected and locally finite. Let  $d$  represent the distance metric on  $G$ , where  $d(i, j)$  denotes the length of the shortest path from node  $i$  to node  $j$ . In addition, let  $\delta_k(i)$  be the  $k$ -path degree of node  $i$ , indicating the number of nodes at a distance of  $k$  from  $i$ .

$$\delta_k(i) = \#\{j \in V \mid d(i, j) = k\}. \quad (5)$$

The definition of the  $k$ -path Laplacian matrix can be stated without loss of generality, as given in [9].

$$\mathbf{L}_k(i, j) = \begin{cases} \delta_k(i), & \text{if } i = j, \\ -1, & \text{if } d(i, j) = k, \\ 0, & \text{otherwise,} \end{cases} \quad (6)$$

$\delta_k(i)$  can also be seen as the number of irreducible shortest-paths of length  $k$  having node  $i$  as end point [9]. The  $k$ -path Laplacian matrices naturally extend the combinatorial Laplacian of a graph. When  $k = 1$ , the path Laplacian matrix defined by (6) is simply the traditional Laplacian matrix. The notion of the  $k$ -path Laplacian has been broadened to include connected and locally finite graphs [15]. The  $k$ -path Laplacian matrices naturally extends the concept of graph connectivity to  $k$ -connectivity. It determines whether every node in the graph can be reached by a particle undergoing  $k$ -hopping from one node to another. As demonstrated in [15], the path Laplacian matrix  $\mathbf{L}_k$  can be viewed as an operator on the set of square-summable functions  $l^2(V)$ . In

addition, it is established as a self-adjoint and non-negative operator.

*Definition 1* ( $k$ -hopping walk). A  $k$ -hopping walk of length  $l$  is defined as any sequence of nodes  $v_1, v_2, \dots, v_l, v_{l+1}$  where  $d_{i,i+1} = k$  for each  $i = 1, 2, \dots, l$ . In simpler terms, this walk is referred to as a  $k$ -hopping walk from  $v_1$  to  $v_{l+1}$  [9].

$$\mathbf{L}_1(G) = \begin{pmatrix} 2 & -1 & 0 & -1 \\ -1 & 3 & -1 & -1 \\ 0 & -1 & 2 & -1 \\ -1 & -1 & -1 & 3 \end{pmatrix}, \mathbf{L}_2(G) = \begin{pmatrix} 1 & 0 & -1 & 0 \\ 0 & 0 & 0 & 0 \\ -1 & 0 & 1 & 0 \\ 0 & 0 & 0 & 0 \end{pmatrix}, \mathbf{L}_3(G) = \begin{pmatrix} 0 & 0 & 0 & 0 \\ 0 & 0 & 0 & 0 \\ 0 & 0 & 0 & 0 \\ 0 & 0 & 0 & 0 \end{pmatrix}. \quad (7)$$

As shown in [9], it has been demonstrated that the  $k$ -path Laplacian matrices are positive semi-definite and satisfy the following condition:

$$\mathbf{y}^T \mathbf{L}_k \mathbf{y} \geq 0, \quad \forall \mathbf{y} \in \mathbb{R}^n \setminus \{\mathbf{0}\}. \quad (8)$$

The equality holds true for any vector  $\mathbf{y}$  in the eigenspace  $\mathbf{L}_k$  corresponding to the eigenvalue  $\lambda_1(\mathbf{L}_k) = 0$ .

*Definition 2* ( $k$ -hopping connected component). A  $k$ -hopping connected component of a graph  $G = (V, E)$  refers to a subgraph  $G' = (V', E')$ , where  $V' \subset V$  and  $E' \subset E$ , and it is characterized by the presence of at least one  $k$ -hopping walk that traverses every node  $v_i \in V'$ .

*Example 1.* Consider the graph  $G$  shown in Figure 1. Given that  $d_{\max} = 2$ , we proceed to calculate the 1-hopping and 2-hopping connected components of  $G$ .

From Table 2, it is evident that when examining hops of length  $k = 1$ , there exists a single connected component, corresponding to the multiplicity of 0 as an eigenvalue in the spectrum denoted as 0, 2, 4, and 4. Conversely, when considering hops of length 2 ( $k = 2$ ), three components emerge, mirroring the multiplicity of 0 as an eigenvalue in the associated spectrum 0, 0, 0, and 2. Further insights into  $k$ -path Laplacian matrices can be found in [9].

### 3. Generalized Heat Kernel

Let us now consider the heat diffusion process on the graph  $G$  of the form

$$\frac{d\mathbf{u}}{dt} = -\mathbf{L}_G \mathbf{u}; \quad \mathbf{u}(0) = \mathbf{u}_0, \quad (9)$$

where the operator  $\mathbf{L}_G$  also called here the generalized Laplacian is given by the series

$$\mathbf{L}_G = \sum_{k=1}^{\infty} c_k \mathbf{L}_k, \quad (10)$$

In the case of the simple graph depicted in Figure 1 with a diameter equal to 2, the  $k$ -degree ( $k \leq 2$ ) for each vertex is presented in Table 1. For illustration purpose, let's calculate the  $k$ -path Laplacian matrices for the simple of Figure 1. It is noteworthy that, given that the maximum distance  $d_{\max}$  in the graph is 2, we can only consider  $k = 1$  and  $k = 2$ . Therefore, the resulting  $k$ -path Laplacian matrices are given by:

with  $c_k \in \mathbb{C}$ . Estrada et al. [15] show that if the operators  $\mathbf{L}_k$  are bounded and

$$\sum_{k=1}^{\infty} |c_k| \|\mathbf{L}_k\| < \infty, \quad (11)$$

then, the series (10) converges to a bounded operator in  $l^2(V)$ . When the graph is finite we simply write

$$\mathbf{L}_G = \sum_{k=1}^{d_{\max}} c_k \mathbf{L}_k, \quad (12)$$

where  $d_{\max}$  represents the diameter of the graph  $G$ . The coefficients  $c_k$  hold a pivotal significance in extending the diffusion process on networks, making it essential to ascertain their values. The expected behavior of the coefficients  $c_k$  is to assign greater weight to shorter paths compared to longer-range interactions. Determining the appropriate values of  $c_k$  is therefore a crucial task in optimizing the generalization of the diffusion process.

In this context, when considering diffusion equation (9) the heat kernel on a finite graph/network is given by

$$\mathbf{H}(t) = \exp(-t\mathbf{L}_G) = \exp\left(-t \sum_{k=1}^{d_{\max}} c_k \mathbf{L}_k\right). \quad (13)$$

The kernel (13) extends kernel (4) which is discussed at length in [19]. The expression (13) is called  $k$ -path Laplacian-based heat kernel or the generalized heat kernel with long-range interactions (LRI). It describes the flow of heat/information not only along the edges (or between adjacent nodes) but also allows heat transfer by long-range jumps (long-range interactions) between nodes that are not adjacent. When  $c_k = 1$  and  $c_{k>2} = 0$  we recover (4) based on the Laplacian matrix  $\mathbf{L}$  which describes the flow of heat only via adjacent nodes. Before this paper, the heat kernel (13) was not studied in the literature. This new kernel based on  $k$ -path Laplacian matrices is the main focus of this paper.

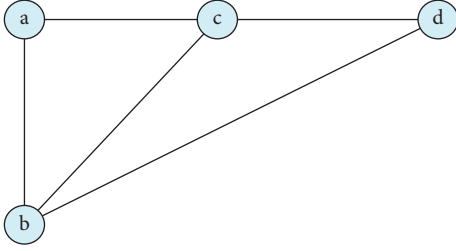


FIGURE 1: A simple graph.

TABLE 1:  $k$ -path degree for vertices of graph in Figure 1.

Vertex	$\delta_1$	$\delta_2$
<i>a</i>	2	1
<i>b</i>	3	0
<i>c</i>	3	0
<i>d</i>	2	1

TABLE 2: Computation of  $k$ -hopping connected components of the graph depicted in Figure 1.

	No. of components		Components
$\lambda_i(\mathbf{L}_1)$	<b>0</b>	1	a-b-c-d
	2		
	4		
	4		
$\lambda_i(\mathbf{L}_2)$	<b>0</b>	3	a-c b d
	<b>0</b>		
	<b>0</b>		
	2		

The number of zero(s) (in bold) as eigenvalue corresponds to the number of  $k$ -hopping connected components in the graph/network.

The coefficient  $c_k$  must be chosen such that the interactions between nodes at a large distance are penalized than nodes at a shorter distance. These considerations are taken into account by applying Laplace and Mellin transforms, as explained in [9]. An analogous approach was employed in [14] to devise a methodology for addressing long-range interactions (LRI) between a designated pair of nodes separated by a distance  $k$ . This method involves assigning weights that consider the principle that as the separation distance increases, the influence of LRI weakens. In the Laplace transform, the rate at which LRI weakens with an increase in distance  $d$  follows an exponential decay. Consequently, using the Laplace transform of the  $k$ -path Laplacian matrices yields:

$$\mathbf{L}_G = \mathbf{L} + \sum_{k=2}^{\infty} e^{-\lambda k} \mathbf{L}_k, \quad (14)$$

where the coefficients in (12) are  $c_1 = 1$  and  $c_{k \geq 2} = e^{-\lambda k}$  with  $\lambda > 0$ . In the case of the Mellin transform, the decay behavior follows a power law, characterized by  $k^{-s}$  where  $s > 0$ . We can then write

$$\mathbf{L}_G = \sum_{k=1}^{\infty} k^{-s} \mathbf{L}_k, \quad (15)$$

where are  $c_k = k^{-s}$ . Normal diffusion takes place exclusively when  $s > 3$ , whereas superdiffusion occurs within the range  $1 < s < 3$  [15]. With the specified coefficients  $c_k$ , the generalized heat kernel (13) for a finite graph/network, incorporating both direct interactions and long-range interactions (LRI) modeled through Laplace or Mellin transforms, can be expressed as follows:

$$\mathbf{H}(t) = \begin{cases} \exp \left[ -t \left( \mathbf{L} + \sum_{k=2}^{\Delta} e^{-\lambda k} \mathbf{L}_k \right) \right], & \text{Laplace } \lambda > 0, \\ \exp \left[ -t \left( \sum_{k=1}^{\Delta} k^{-s} \mathbf{L}_k \right) \right], & \text{Mellin } s > 0, \end{cases} \quad (16)$$

where  $\lambda$  and  $s$  stand for positive constant parameters associated with the Laplace and Mellin transforms, respectively, while  $1 \leq \Delta \leq d_{\max}$ . We will use (16) for graph characterization using various values of  $\lambda$  for the Laplace and  $s$  Mellin transform. In addition, we will explore the impact of the network structure on this quantity and its invariants. The heat kernel (16), involving  $k$ -path Laplacian matrices, can be visualized as a matrix of size  $|V| \times |V|$ . For nodes  $p$  and  $q$  in the graph  $G$ , the corresponding element is

$$\mathbf{H}_t(p, q) = \sum_{i=1}^{|V|} \exp(-\lambda_i t) \mathbf{v}_i(p) \mathbf{v}_i(q), \quad (17)$$

where  $\lambda_i$  is the generalized eigenvalue associated with generalized eigenvector  $\mathbf{v}_i$  of the matrix  $\mathbf{L}_G$  either for the Laplace or Mellin transform.

Figure 2 gives a simple diagrammatic illustration of the direct diffusion model (left) and the long-range interaction model (right). Our generalized heart kernel (16) captures the configuration in (b) where diffusion is allowed to hop for example between node 3 and node 1 at distance 2 and between node 4 and node 1 at distance 3 in the network. The traditional Laplacian  $\mathbf{L}$  captures situation (a) in which diffusion is only allowed between adjacent nodes. It is clear that the hear kernel (16) naturally generalize the heat kernel (4). Unless otherwise specified we will be interested in the normalized version of the operator  $\mathbf{L}_G$ , which is

$$\hat{\mathbf{L}}_G = \mathbf{D}_G^{-1/2} (\mathbf{D}_G - \mathbf{A}_G) \mathbf{D}_G^{-1/2} = \mathbf{I} - \mathbf{D}_G^{-1/2} \mathbf{A}_G \mathbf{D}_G^{-1/2}, \quad (18)$$

where  $\mathbf{D}_G$  is the generalized degree matrix (i.e. a matrix whose diagonal has the generalized degrees of nodes) and  $\mathbf{A}_G$  the generalized adjacency matrix. For example for the Mellin transform these matrices are given by

$$\mathbf{A}_G = \sum_{k=1}^{d_{\max}} k^{-s} \mathbf{P}_k, \quad (19)$$

$$\mathbf{D}_G = \sum_{k=1}^{d_{\max}} k^{-s} \mathbf{\Delta}_k,$$

where the  $k$ -path (adjacency) matrix  $\mathbf{P}_k$  and the  $k$ -path degree matrix  $\mathbf{\Delta}_k$  are given as in [9]:

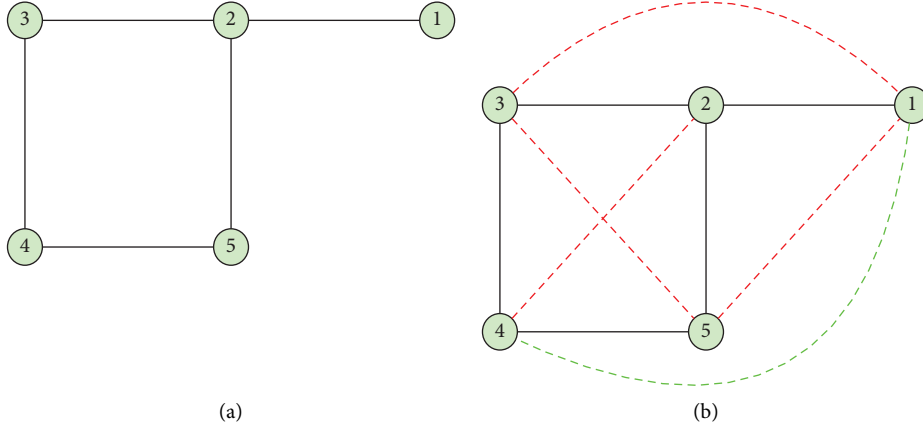


FIGURE 2: A simple graph indicating the direct interactions which characterized the normal diffusion model (a). A simple graph indicating both direct interactions (black solid lines) and LRI at hops of length 2 (red broken lines) and length 3 (green-broken lines) that depict the generalized diffusion model (b).

$$\mathbf{P}_k = \begin{cases} 1, & \text{if } d(i, j) = k, \\ 0, & \text{otherwise,} \end{cases} \quad (20)$$

$$\Delta_k = \text{diag}(\mathbf{1}^T \mathbf{P}_k),$$

where  $\mathbf{1}$  denotes an all-ones column vector. For illustration, the generalized adjacency  $\mathbf{A}_G$  and degree matrices  $\mathbf{D}_G$  obtained using the Mellin transform of the  $k$ -path Laplacian matrix of the graph in Figure 2(a) are, respectively, given by

$$\mathbf{A}_G = \begin{pmatrix} 0 & 1 & \frac{1}{2^s} & \frac{1}{3^s} & \frac{1}{2^s} \\ 1 & 0 & 1 & \frac{1}{2^s} & 1 \\ \frac{1}{2^s} & 1 & 0 & 1 & \frac{1}{2^s} \\ \frac{1}{3^s} & \frac{1}{2^s} & 1 & 0 & 1 \\ \frac{1}{2^s} & 1 & \frac{1}{2^s} & 1 & 0 \end{pmatrix}, \mathbf{D}_G = \begin{pmatrix} \frac{1}{3^s} + 2^{1-s} + 1 & 0 & 0 & 0 & 0 \\ 0 & \frac{1}{2^s} + 3 & 0 & 0 & 0 \\ 0 & 0 & 2^{1-s} + 2 & 0 & 0 \\ 0 & 0 & 0 & \frac{1}{3^s} + \frac{1}{2^s} + 2 & 0 \\ 0 & 0 & 0 & 0 & 2^{1-s} + 2 \end{pmatrix}, \quad (21)$$

and the generalized Laplacian matrix (not normalized) when using the Mellin transform is

$$\mathbf{L}_{\text{Mellin}} = \begin{pmatrix} \frac{1}{3^s} + 2^{1-s} + 1 & -1 & \frac{1}{2^s} & \frac{1}{3^s} & -\frac{1}{2^s} \\ -1 & \frac{1}{2^s} + 3 & -1 & -\frac{1}{2^s} & -1 \\ \frac{1}{2^s} & -1 & 2^{1-s} + 2 & -1 & -\frac{1}{2^s} \\ \frac{1}{3^s} & \frac{1}{2^s} & -1 & \frac{1}{3^s} + \frac{1}{2^s} + 2 & -1 \\ \frac{1}{2^s} & -1 & \frac{1}{2^s} & -1 & 2^{1-s} + 2 \end{pmatrix}, \quad (22)$$

and the normalized version can be computed using the formula (18). We observe that  $\lim \mathbf{A}_G = \mathbf{A}$ ,  $\lim \mathbf{D}_G = \mathbf{D}$ , and  $\lim \mathbf{L}_{\text{Mellin}} = \mathbf{L}$  when  $s \rightarrow \infty$ , i.e., when there is no long-range interactions. With this matrix, the generalized heart kernel derived from the Mellin transforms of  $k$ -path Laplacian can be written down using equation (16). We can also observe that  $\lim \mathbf{L}_{\text{Laplace}} = \mathbf{L}$  when  $\lambda \rightarrow \infty$ . The following lemma is self-evident.

**Lemma 3.** *The generalized Laplacian matrix  $\mathbf{L}_G$  given in (12) is symmetric and positive semidefinite and hence its generalized eigenvalues are all non-negative; furthermore  $\mathbf{L}_G$  has zero as an eigenvalue with  $\mathbf{1}$  as the corresponding eigenvector.*

This results from the fact that the generalized Laplacian matrix  $\mathbf{L}_G$  is a linear combination of  $k$ -path Laplacian matrices each of which is symmetric, positive semidefinite, and has  $\mathbf{1}$  as eigenvector with zero as eigenvalue [9]. The results of Lemma 3 also hold for the generalized normalized Laplacian matrix  $\hat{\mathbf{L}}_G$  whose spectral decomposition is given by  $\hat{\mathbf{L}}_G = \mathbf{V}\mathbf{\Lambda}\mathbf{V}^T$ , where  $\mathbf{\Lambda} = \text{diag}(\lambda_1, \lambda_2, \dots, \lambda_{|V|})$  is the matrix with the ordered eigenvalues ( $\lambda_1 \leq \lambda_2 \leq \dots \leq \lambda_{|V|}$ ) as elements and  $\mathbf{V} = (\mathbf{v}_1 | \mathbf{v}_2 | \dots | \mathbf{v}_{|V|})$  is the matrix with the ordered eigenvectors as columns. A notable distinction between the spectra of  $\mathbf{L}_G$  and  $\hat{\mathbf{L}}_G$  lies in the fact that the eigenvalues of the former can be essentially as large as desired, particularly ranging from 0 to twice the maximum degree. In contrast, the latter has eigenvalues always confined to the range between 0 and 2, inclusive, as demonstrated in [26]. This presents an advantage, as the normalized version  $\hat{\mathbf{L}}_G$  of  $\mathbf{L}_G$  facilitates easier comparison of eigenvalue distributions across different graphs, especially when there is a substantial difference in graph sizes. The normalized Laplacian is linked to numerous interesting graph properties [27].

**Lemma 4.** *Let  $G = (V, E)$  be a graph/network and  $\mathbf{L}_G$  and  $\mathbf{L}'_G$  be, respectively, its generalized Laplacian matrices with Laplace and Mellin transforms of its  $k$ -path Laplacian matrices as defined in equations (14) and (15) and let  $\lambda_i$  and  $\lambda'_i$  be the corresponding eigenvalues, then we have  $\mathbf{L}_G \leq \mathbf{L}'_G$  for  $\lambda = s > 0$  and  $\lambda_i \leq \lambda'_i$ ,  $i = 1, \dots, n$  and  $k = 1, \dots, d_{\max}$  as illustrated in Figure 3.*

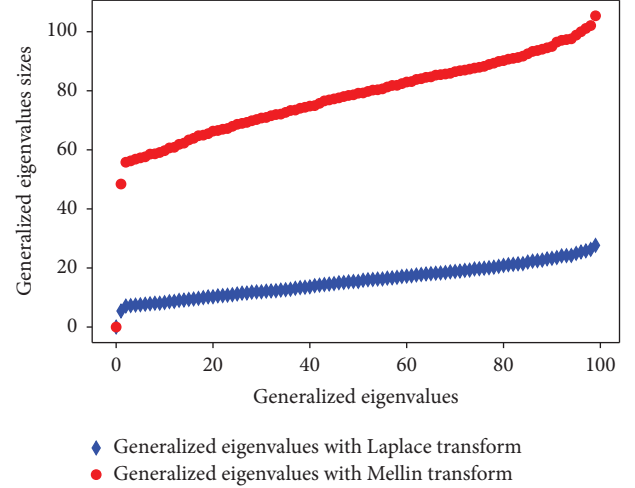


FIGURE 3: Illustration of the result of Lemma 4. We consider a Gilbert model  $G(n, p)$  for random graphs with  $n = 100$  nodes and connection probability  $p = 0.07$  (connected regime) generated using NetworkX [28] in Python. We then plot the generalized eigenvalues of the corresponding generalized Laplacian matrices (14) and (15) for  $\lambda = s = 0.5$ . We observe that the eigenvalues of the generalized Laplacian matrix with the Mellin transform are greater (apart from  $\lambda_1 = 0$ , where they equal) compared to the corresponding eigenvalues of the generalized Laplacian matrix with Laplace transform.

*Proof.* First of all, it is easy to see that  $e^{-\lambda k} \leq k^{-s}$  for  $\lambda = s > 0$ , with equality when  $\lambda, s \rightarrow \infty$ . This implies that  $\mathbf{L}_G \leq \mathbf{L}'_G$ . On the other hand, using the Rayleigh quotients  $R_{\mathbf{L}_G}$  and  $R_{\mathbf{L}'_G}$  of matrices  $\mathbf{L}_G$  and  $\mathbf{L}'_G$ , we have the following for any vector  $\mathbf{x} \neq \mathbf{0}$ :

$$\begin{aligned} \mathbf{L}_G &\leq \mathbf{L}'_G, \\ \mathbf{x}^T \mathbf{L}_G \mathbf{x} &\leq \mathbf{x}^T \mathbf{L}'_G \mathbf{x}, \\ R_{\mathbf{L}_G}(\mathbf{x}) &= \frac{\mathbf{x}^T \mathbf{L}_G \mathbf{x}}{\mathbf{x}^T \mathbf{x}} \leq R_{\mathbf{L}'_G}(\mathbf{x}) = \frac{\mathbf{x}^T \mathbf{L}'_G \mathbf{x}}{\mathbf{x}^T \mathbf{x}}, \\ \lambda_1 &= \min_{\mathbf{x} \neq \mathbf{0}} R_{\mathbf{L}_G}(\mathbf{x}) \leq \lambda'_1 = \min_{\mathbf{x} \neq \mathbf{0}} R_{\mathbf{L}'_G}(\mathbf{x}), \\ \lambda_n &= \max_{\mathbf{x} \neq \mathbf{0}} R_{\mathbf{L}_G}(\mathbf{x}) \leq \lambda'_n = \max_{\mathbf{x} \neq \mathbf{0}} R_{\mathbf{L}'_G}(\mathbf{x}). \end{aligned} \quad (23)$$

By using the max-min theorem we have for any other eigenvalues:

$$\begin{aligned} \lambda_k &= \min_U \left\{ \max_{\mathbf{x}} \{ R_{\mathbf{L}_G}(\mathbf{x}) \mid \mathbf{x} \in U \text{ and } \mathbf{x} \neq \mathbf{0} \} \mid \dim(U) = k \right\} \\ &\leq \lambda'_k = \min_U \left\{ \max_{\mathbf{x}} \{ R_{\mathbf{L}'_G}(\mathbf{x}) \mid \mathbf{x} \in U \text{ and } \mathbf{x} \neq \mathbf{0} \} \mid \dim(U) = k \right\}. \end{aligned} \quad (24)$$

□

## 4. Generalized Heat Kernel Invariants

In this section, we will extract meaningful invariants from the generalized heat kernel and leverage them for graph characterization.

**4.1. Trace of the Generalized Heat Kernel.** The trace of the generalized heat kernel at time  $t$ , denoted as  $\text{Tr}(\mathbf{H}_t)$ , is the sum of the entries at the main diagonal of the matrix  $\mathbf{H}_t$ . In other words, it is given by

$$Z(t) = \text{Tr}(\mathbf{H}_t) = \text{Tr}(\mathbf{V} \exp(-t\mathbf{\Lambda}) \mathbf{V}^T) = \sum_i^{|\mathbf{V}|} \exp(-\lambda_i t). \quad (25)$$

It remains invariant under node label permutations and is a function whose parameters include the eigenvalues of the generalized Laplacian matrix  $\hat{\mathbf{L}}_G$ , with time as its argument. For a connected graph, the expression is given by

$$Z(t) = 1 + e^{-\lambda_2 t} + e^{-\lambda_3 t} + \dots + e^{-\lambda_{|\mathbf{V}|} t}. \quad (26)$$

Equation (26) generalizes an equation from [19] by including the effect of long-range interaction. We can also write

$$\text{Tr}(\mathbf{H}_t) = C + \sum_{\lambda_i \neq 0}^{|\mathbf{V}|} e^{-\lambda_i t}, \quad (27)$$

where  $C$  is the number of connected components of the network which is also the multiplicity of zero as eigenvalue of  $\hat{\mathbf{L}}_G$ .

**Lemma 5.** *Let  $G = (V, E)$  be a graph/network and let  $Z(t)$  and  $Z'(t)$  be, respectively, the trace of the generalized heat kernel of  $G$  for the Laplace and Mellin transform-based cases for  $\lambda = s$ . Then, we have  $Z(t) \geq Z'(t)$  with equality when  $t = 0$  and  $t \rightarrow +\infty$ .*

Lemma 5 follows immediately from Lemma 4. In other words, Lemma 5 states that the stronger the long-range interactions, the weaker the contribution of the corresponding trace of the generalized heat kernel.

In spectral geometry, various invariants of the Riemannian manifold can be extracted by estimating the heat kernel [26]. In the majority of literature, the focus is often on the trace of the heat kernel rather than the heat kernel itself. This preference arises from the fact that the trace, as shown in (25), captures the essential aspects of the heat kernel and can be computed in polynomial time. In essence, using the trace helps simplify the computation of the heat kernel, making it an efficient tool for capturing graph properties and key invariants. For instance, in a complete graph such as  $K_4$ , the entry  $\mathbf{H}_t(p, p)$  is the same for all vertices  $p$ , facilitating the computation of the trace.

**4.1.1. Graph Characterization Using the Heat Kernel Trace.** The heat kernel trace serves as a valuable tool for distinguishing graphs with different typologies, relying on the characteristic shapes of the heat kernel trace curves over time, as discussed in [19]. To illustrate this concept, we examine three simple graphs: a star, a path, and a 2-regular graph, each with a size of 10. Figure 4 depicts plots of the heat kernel trace (without considering LRI) against time for these three graphs.

From the observations in Figure 4, it is apparent that the three graphs with different topologies exhibit distinct and varied shapes in their corresponding heat kernel trace curves. Notably, the curves for the path graph and the 2-regular graph (ring) are relatively close to each other due to their similar topology. In contrast, the curve corresponding to the star graph is notably distinct, characterized by a different shape with a deeper trough.

**4.1.2. Trace of the Generalized Heat Kernel Experiment.** We are now interested in determining whether the trace of the generalized heat kernel can serve as a tool for graph characterization, similar to the trace of the standard heat kernel discussed earlier. Let's consider the graphs shown in Figure 4(b), and in Figure 5, we plot the trace functions at each time step  $t$  for the generalized Laplacian matrix based on both the Mellin and Laplace transforms of the  $k$ -path Laplacian matrices.

From the observations in Figure 5, we notice distinct curves with different shapes for the trace of the heat kernel, both for the standard and generalized Laplacian matrices, across the three graphs. In the case of the Mellin transform-based generalized trace function (middle row), when  $s = 2$  (Figure 5(b)), the curves become closer to each other. However, their distinctiveness is still evident, although their slopes differ slightly. For  $s = 3$  (Figure 5(c)), the curves corresponding to the three graphs are much more distinct, and their shape tends to resemble the trace plot of the standard Laplacian matrix (see Figure 5(a)). This phenomenon can be attributed to a decrease in the strength of long-range interactions (LRI) as  $s$  increases. In the Laplace transform-based cases (bottom row) (see Figures 5(d) and 5(e)), we observe similar behavior to the Mellin transform-based case, with the curves becoming more distinct as the values of  $\lambda$  increase. The observed difference in behavior, where the trace plots in the Laplace transform-based case tend to converge more rapidly to the trace plots of the standard Laplacian matrix as  $s$  and  $\lambda$  increase, can be attributed to the stronger long-range influence in the Mellin transform-based case compared to the Laplace transform-based case for the same values of the respective exponents (Lemma 5). Thus, as the values of the exponents increase, there is a decrease in long-range influence with the rate of decrease much faster in the Laplace than the Mellin-based case. Hence, with an increase in the values of the exponents, there is a reduction in long-range influence, and this reduction occurs at a faster rate in the Laplace transform-based case compared to the Mellin transform-based case which explains the fast tendency of the corresponding trace function to the trace function of the standard diffusion model in the former than in the latter case. The plots clearly demonstrate that the trace function of the generalized heat kernel is a valuable tool for analyzing graphs with different topologies. Now, let's delve into a simple toy example to illustrate how the trace of the generalized heat kernel varies with time for different values of the Mellin exponent  $s$  and Laplace exponent  $\lambda$ .

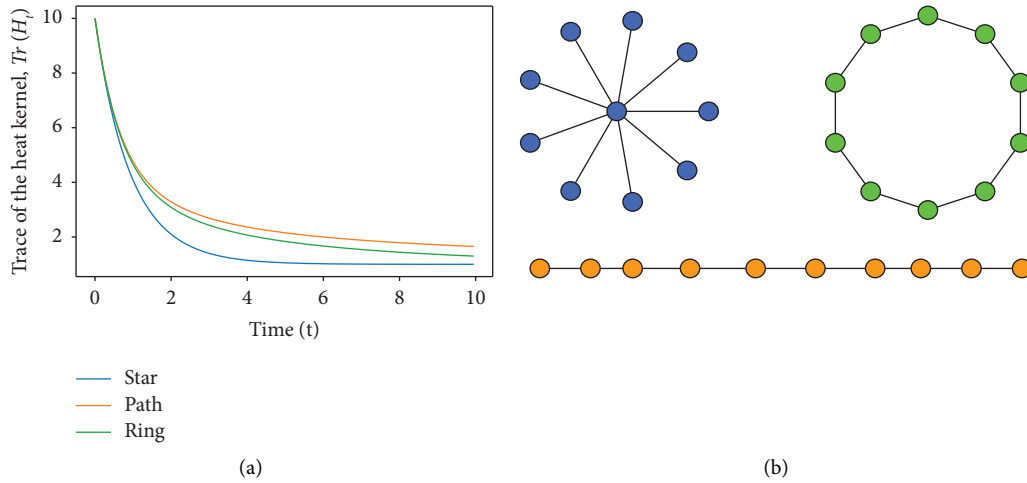


FIGURE 4: Heat kernel trace curves when there is no LRI (a) for three different graphs: star (blue), path (orange), and regular (green) graphs having 10 nodes (b).

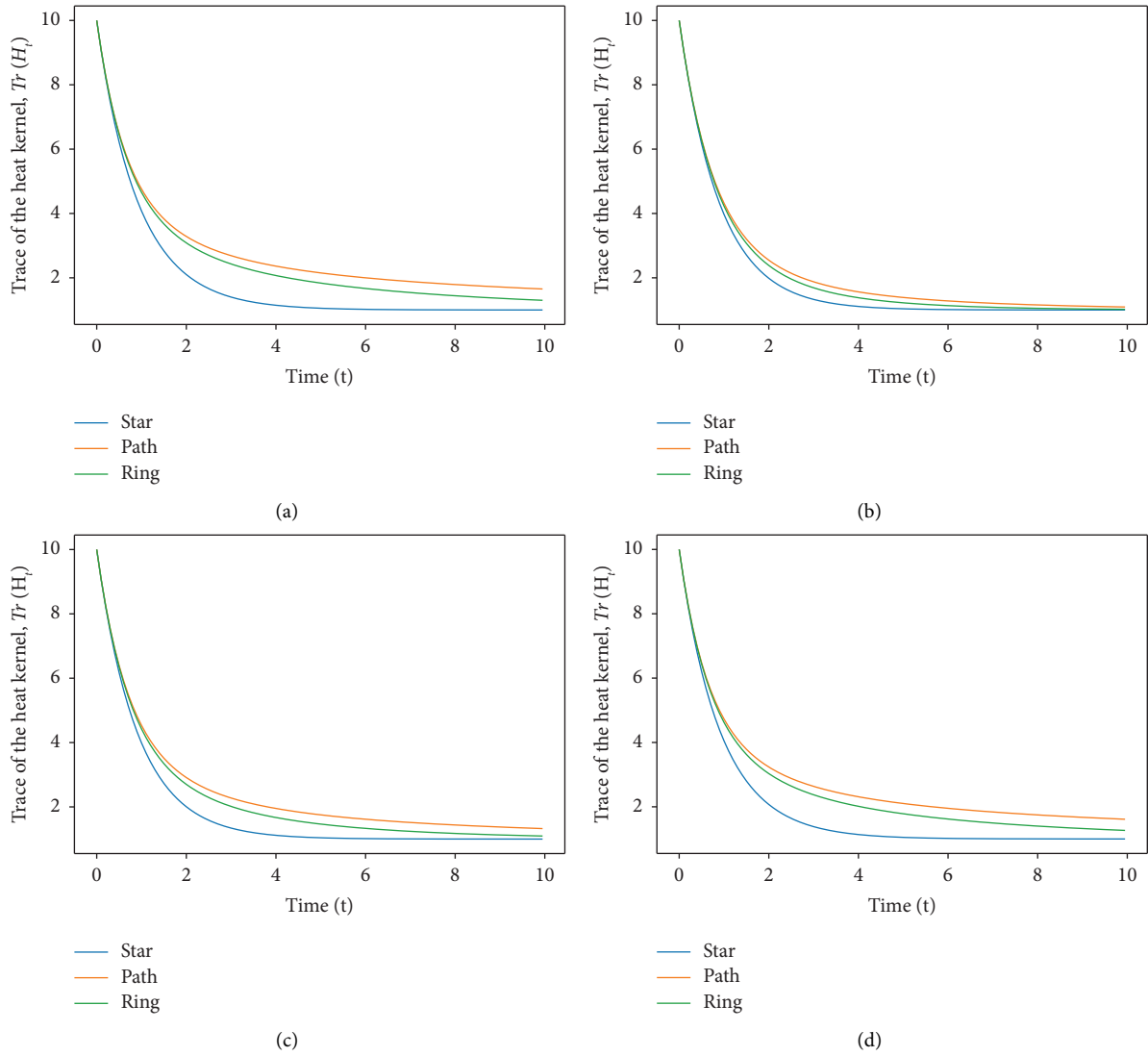
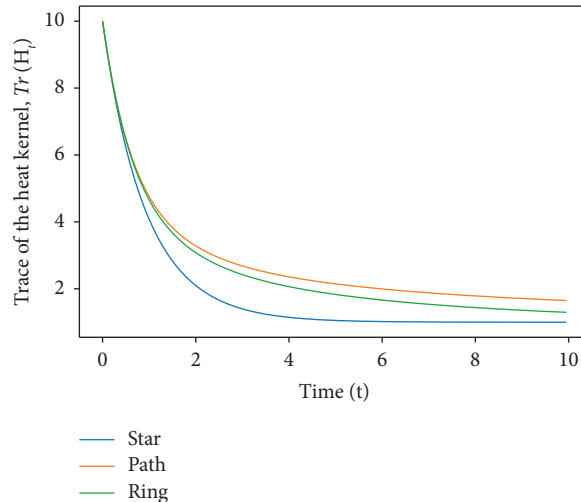


FIGURE 5: Continued.



(e)

FIGURE 5: Plots of the trace of the generalized heat kernel against time for the star (blue curve), ring (green curve), and path (orange curve) graphs of Figure 4(b). For comparison purposes, subfigure (a) shows the plot of the trace of the standard heat kernel. Subfigures (b) and (c) correspond to plots of the trace function for the generalized heat kernel based on the Mellin transform with  $s = 2$  and  $s = 3$ , respectively. Subfigures (d) and (e) are plots of trace function of the generalized heat kernel based on Laplace transform for  $\lambda = 2$  and  $\lambda = 3$ , respectively. As can be seen, for the same values of  $\lambda$  and  $s$ , the trace function based on the Mellin transform decreases faster than that for the Laplace transform-based function. This fact is justified by the claim of Lemma 5.

In Figure 6, it is noticeable that the trace function curve against time for diffusion along edges (referred to as direct interactions) of the graph (depicted in blue) is positioned at the uppermost level and gradually decreases over time. When considering long-range influence, it becomes evident that as the parameters  $\lambda$  and  $s$  for the Laplace and Mellin transforms increase, the respective curves tend to converge towards the one representing standard diffusion (in blue).

However, the convergence to the standard curve occurs more rapidly in the Laplace transform-based case than in the Mellin transform-based case. This discrepancy is explained by the stronger long-range influence in the Mellin case compared to the Laplace case for the same values of power exponents. Specifically, for  $\lambda = s = 3.0$  (depicted in brown), it can be observed from Figure 6 that the curve corresponding to the Laplace transform-based case coincides with that of the normal Laplacian, while in the Mellin case, the curve is more distant from the curve of the standard Laplacian.

We conclude this section by delving into the case of co-spectral graphs, where the trace of the heat kernel may exhibit certain limitations. Co-spectral graphs, despite not being necessarily isomorphic, share the same multiset of eigenvalues as the corresponding Laplacian matrices. It can be difficult to characterize co-spectral graphs with respect to some matrices. They show similar behavior of the trace function of the heat kernel due to the similarity of eigenvalues. An example of co-spectral graphs for the Laplacian matrix is shown in Figure 8. In Figure 9, we plot the trace of the heat kernel (4) based on the traditional Laplacian  $L$ , the trace of the heat kernel (4) based on the normalized traditional Laplacian  $\mathcal{L}$ , and the trace of the generalized heat kernel (16) based on the normalized form of the Laplace

transform (14) and Mellin transform (15) of the  $k$ -path Laplacian (6) for  $\lambda = 1$  and  $s = 2.3$ .

The graphs in Figure 8 are co-spectral with respect to the traditional Laplacian and also to the Laplace (14) and Mellin transform (15) of the  $k$ -path Laplacian. In this case, as can be seen from Figures 9(a) and 9(b), the trace functions of the kernels (4) and (16) will show the same curve (see the black curve for the kernel (4)) making it difficult to distinguish the 2 graphs. On the other hand, the 2 graphs are not co-spectral with respect to the normalized Laplacian  $\mathcal{L}$  and to the normalized Laplacian of the Laplace and Mellin transforms (14) and (15) of the  $k$ -path Laplacian for  $\lambda = 1$  and  $s = 2.3$ . This time the trace functions of the kernel (4) based on the normalized Laplacian matrices  $\mathcal{L}$  (green and yellow curves) can characterize/distinguish the 2 graphs as one can see from Figures 9(a) and 9(b). This is also true for the trace functions (red and blue curves) of the generalized heat kernel (16) based on the normalized form of the Laplace and Mellin transforms (14) and (15) of the  $k$ -path Laplacian for  $\lambda = 1$  and  $s = 2.3$ .

Considering the general framework of the generalized heat kernel (16), we are able to characterize co-spectral graphs  $G_1$  and  $G_2$  using the trace functions of the generalized heat kernel (16) (based on the normalized version of (14) and (15)) for small value of  $\lambda$  and  $s$ , while we need a very large value(s) of these parameters (when  $\lambda, s \rightarrow \infty$ ) reducing to the trace of the kernel (4) to be able to characterize co-spectral graphs  $G_1$  and  $G_2$ .

We can find non-isomorphic graphs which are co-spectral with respect to the Laplacian matrix and the normalized Laplacian matrix and in this case, the trace functions based on those matrices will not be able to distinguish those graphs. As demonstrated in [27], for sufficiently large  $n$ ,

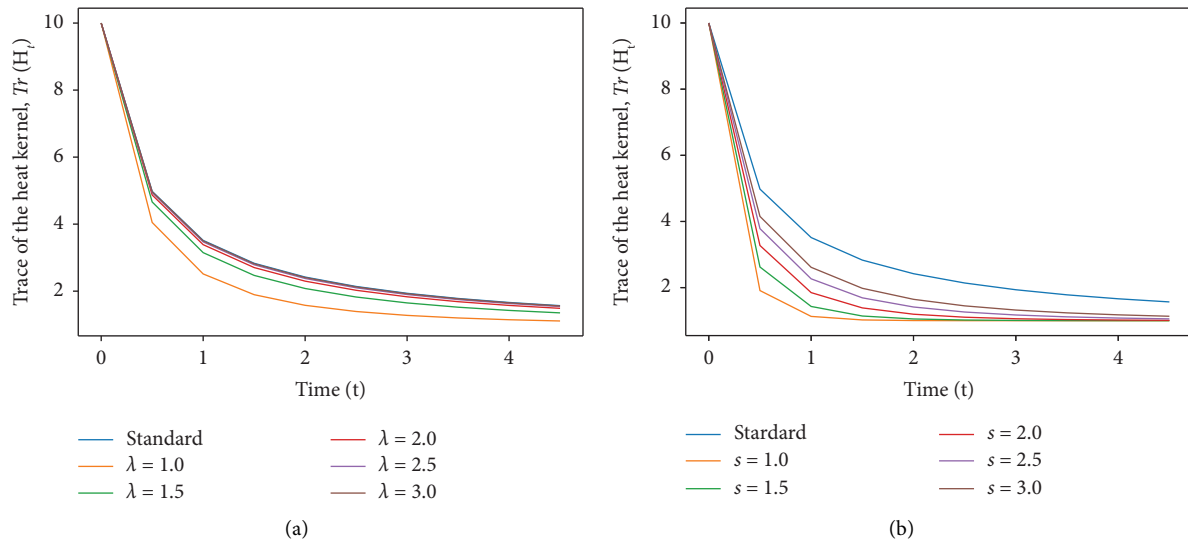


FIGURE 6: Trace of the generalized heat kernel against time for the simple graph in Figure 7. LRI are accounted for by the Laplace (a) and Mellin (b) transforms of the  $k$ -path Laplacian matrix of the graph for different values of  $\lambda$  and  $s$ . By increasing  $\lambda$  and  $s$ , we can see that the traces tend to the trace of the standard Laplacian without no LRI. This is happening much faster when the Laplace transform is used (a) compared to the Mellin transform (b).

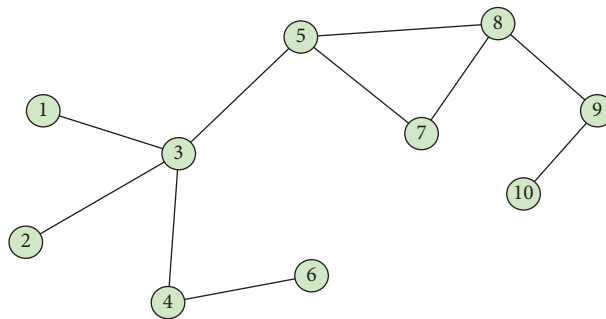


FIGURE 7: A simple network of size 10.

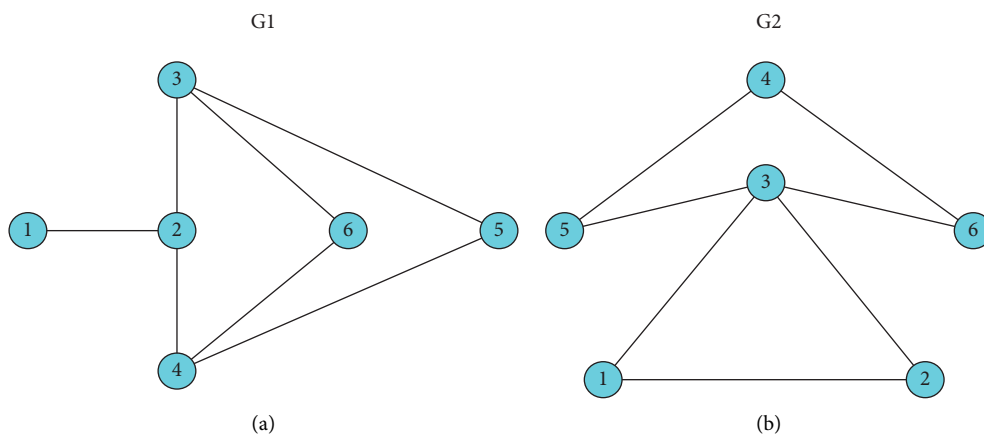


FIGURE 8: The graphs G1 and G2 are co-spectral with respect to the traditional Laplacian  $L$  but not co-spectral when considering the normalized Laplacian  $\mathcal{L}$ . Furthermore, they do not exhibit co-spectrality in relation to the normalized forms of (14) and (15), representing the Laplace and Mellin transforms of the  $k$ -path Laplacian.

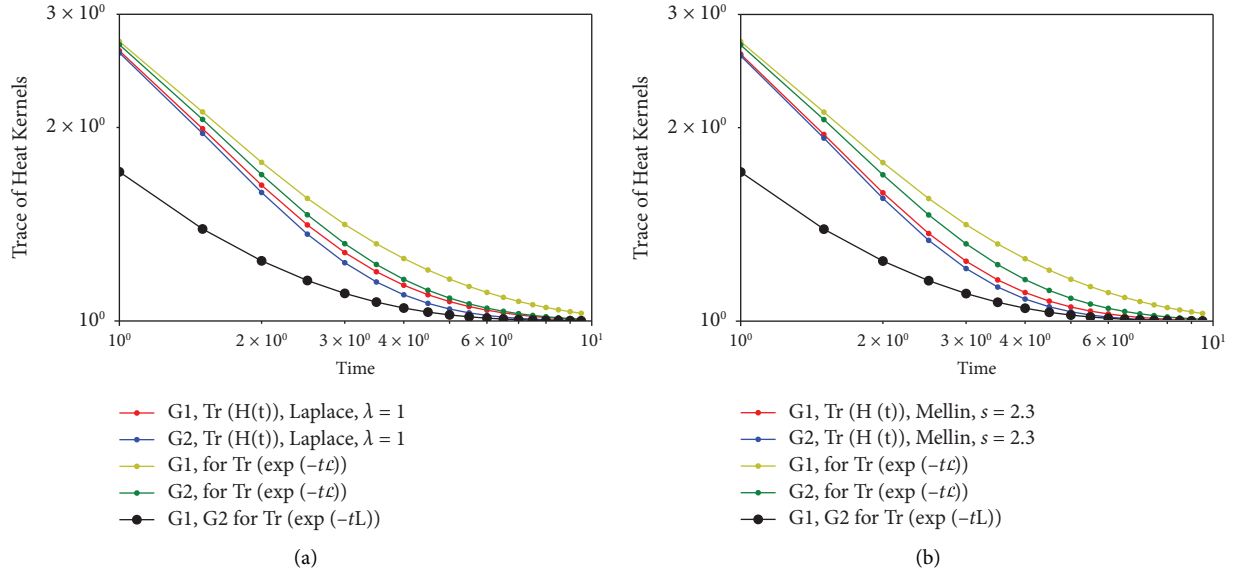


FIGURE 9: Trace functions of the heat kernel (4) based on the normalized Laplacian  $\mathcal{L}$  and the trace functions of the generalized heat kernel (16) based on the normalized form of the Laplace transform (14) and Mellin transform (15) of the  $k$ -path Laplacian for  $\lambda = 1$  and  $s = 2.3$ .

there exists a family of  $2^{\lfloor n/7 \rfloor}$  graphs on  $n$  vertices that are nonisomorphic and mutually co-spectral concerning the normalized Laplacian.

The graphs in Figure 10 are co-spectral with respect to the Laplacian matrix  $\mathbf{L}$  and to the normalized Laplacian matrix  $\mathcal{L}$ , but they are not co-spectral with respect to the Laplace and Mellin transforms of the  $k$ -path Laplacian (14) and (15). In Figure 11, we plot the trace functions of the kernel (4) based on the Laplacian matrix  $\mathbf{L}$  and on the normalized Laplacian matrix  $\mathcal{L}$ . We also plot the trace functions of the generalized heat kernel (16) based on the Laplace and Mellin transforms for  $\lambda = 1.3$  and  $s = 2.3$ . As we can see from Figure 11, the corresponding trace functions (blue and red curves) of the generalized heat kernel (16), based on the Laplace and Mellin transforms, can characterize/distinguish the 2 co-spectral graphs G1 and G2 of Figure 10 while the trace functions of the kernel (4) show only one curve for the 2 graphs when using  $\mathbf{L}$  (black curve) or  $\mathcal{L}$  (green curve). This result is important in the context of the generalized heat kernel (16) based on the Laplace and Mellin transform of the  $k$ -path Laplacian.

**4.2. The Zeta Function.** Several definitions of the zeta function for finite simple graphs exist [29, 30]. In this context, we specifically consider the zeta function associated with the eigenvalues of the generalized Laplacian matrix, which is obtained by exponentiating and summing the reciprocals of the nonzero eigenvalues [30].

$$\zeta(p) = \sum_{\lambda_i \neq 0} \lambda_i^{-p}, \quad (28)$$

where  $\lambda_i$  represents the  $i$ -th eigenvalue of the generalized Laplacian matrix. In the upcoming plot, we examine the behavior of the zeta function against  $p$  for various values of

the Mellin transform exponent  $s$  and Laplace transform exponent  $\lambda$ , considering the graph illustrated in Figure 7.

Examining Figure 12, it is evident that the zeta function exhibits an increasing trend with the exponent  $p$ . For various values of  $\lambda$ , Figure 12(a) illustrates that the zeta function's variation with  $p$  aligns with a pattern similar to that of the standard Laplacian curve (depicted in blue). This similarity arises from a relatively less pronounced long-range influence, which diminishes as the value of  $\lambda$  increases. In contrast, when considering changes in the Mellin exponent  $s$ , noticeable alterations can be observed in the corresponding curves of the zeta function against  $p$  (see Figure 12(b)).

The observed differences in the zeta function curves against  $p$  between the Mellin transform-based and Laplace transform-based cases can be attributed to the more pronounced long-range influence (LRI) in the Mellin transform-based scenario. In the Mellin case, the strength of the long-range influence diminishes as the exponent  $s$  increases. This dynamic explains why the curve corresponding to  $s = 4$  (depicted in purple) tends to align with the shape of the standard zeta function plot (in blue).

**4.3. The Zeta Function and Generalized Heat Kernel Trace Moments.** We investigate the relationship between the generalized heat kernel and the zeta function associated with the eigenvalues of the generalized Laplacian matrix, extending the findings in [19]. To establish this connection, we examine the function  $f(t) = e^{-\lambda t}$ . The Mellin transformation of  $f(t)$  is expressed as follows:

$$F(p) = \int_0^{\infty} t^{p-1} f(t) dt. \quad (29)$$

From the Mellin transform of  $f(t)$  and after little algebraic transformation, we have

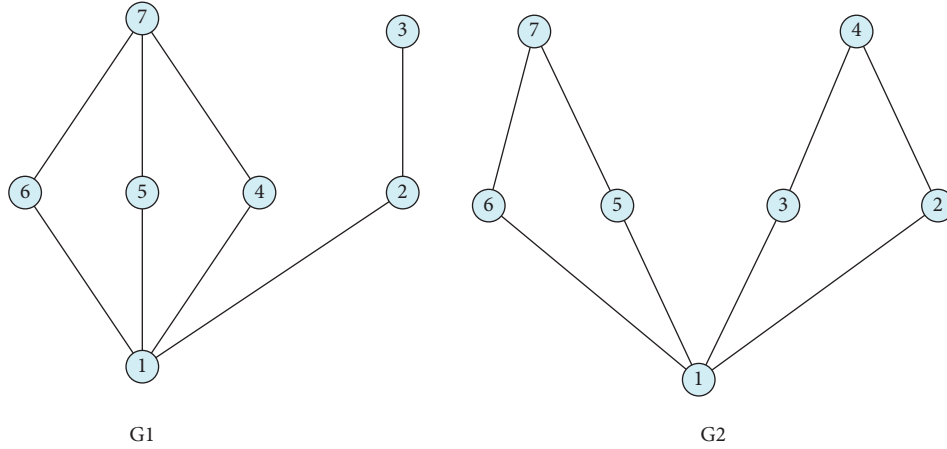


FIGURE 10: Co-spectral graphs G1 and G2 with respect to the Laplacian matrix  $\mathbf{L}$  and to the normalized Laplacian matrix  $\mathcal{L}$ . They are not co-spectral with respect to the Laplace and Mellin transforms of the  $k$ -path Laplacian (14) and (15).

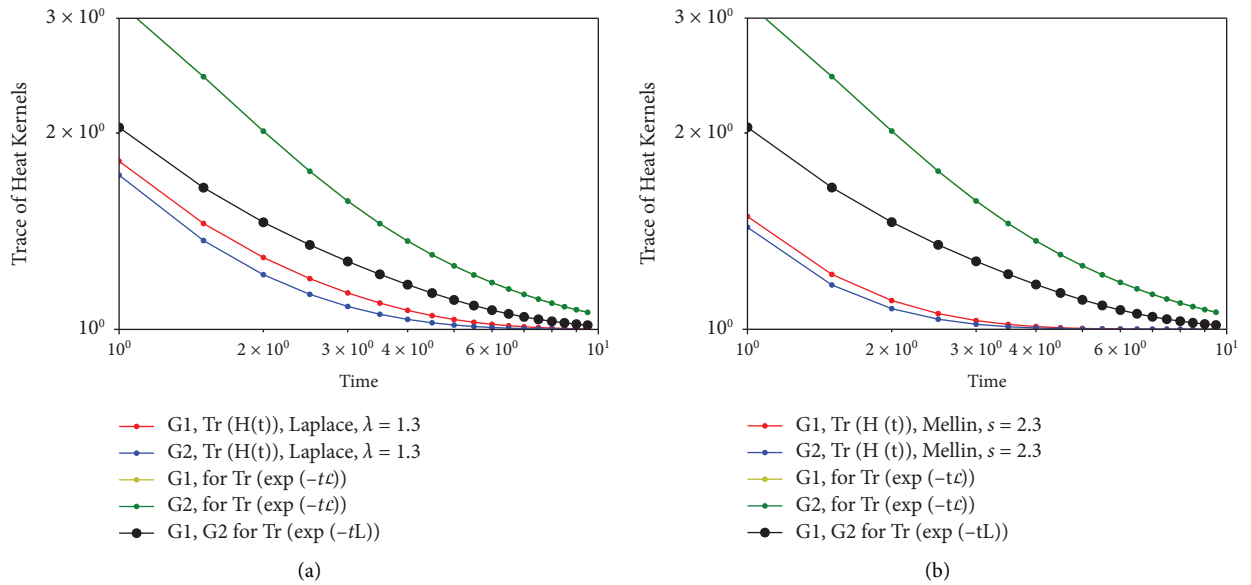


FIGURE 11: Trace functions of the heat kernel (4) based on the matrices  $\mathbf{L}$  and  $\mathcal{L}$  and the trace functions of the generalized heat kernel (16) based on the normalized form of the Laplace transform (14) and Mellin transform (15) of the  $k$ -path Laplacian for  $\lambda = 1.3$  and  $s = 2.3$ .

$$\lambda_i^{-p} = \frac{1}{\Gamma(p)} \int_0^{\infty} t^{p-1} e^{-\lambda_i t} dt, \quad (30)$$

$$\zeta(p) = \frac{1}{\Gamma(p)} \int_0^{\infty} t^{p-1} \{\text{Tr}(\mathbf{H}_t) - C_G\} dt, \quad (33)$$

where  $\lambda_i$  is the  $i$ -th eigenvalue of the generalized Laplacian matrix  $\mathbf{L}_G$ , and  $\Gamma(p)$  represents the gamma function defined as follows:

$$\Gamma(p) = \int_0^{\infty} t^{p-1} e^{-t} dt. \quad (31)$$

Upon summing for all nonzero eigenvalues of the Laplacian, equation (30) transforms into

$$\zeta(p) = \sum_{\lambda_i \neq 0} \lambda_i^{-p} = \frac{1}{\Gamma(p)} \int_0^{\infty} t^{p-1} \sum_{\lambda_i \neq 0} e^{-\lambda_i t} dt. \quad (32)$$

Using the connected component based formula for the trace of the heat kernel, equation (32) becomes

where  $C_G$  represents the number of connected components in the graph. Consequently, the zeta function is intricately linked to the moments of the generalized heat kernel trace. This reveals a profound connection between the zeta function and the moments of the generalized heat kernel trace, offering a comprehensive perspective on the spectral properties of the graph through the lens of both the Laplace and Mellin transforms of the  $k$ -path Laplacian matrices.

**4.4. Derivative of the Zeta Function at the Origin.** The derivative of the zeta function associated with the generalized Laplacian matrix is given by

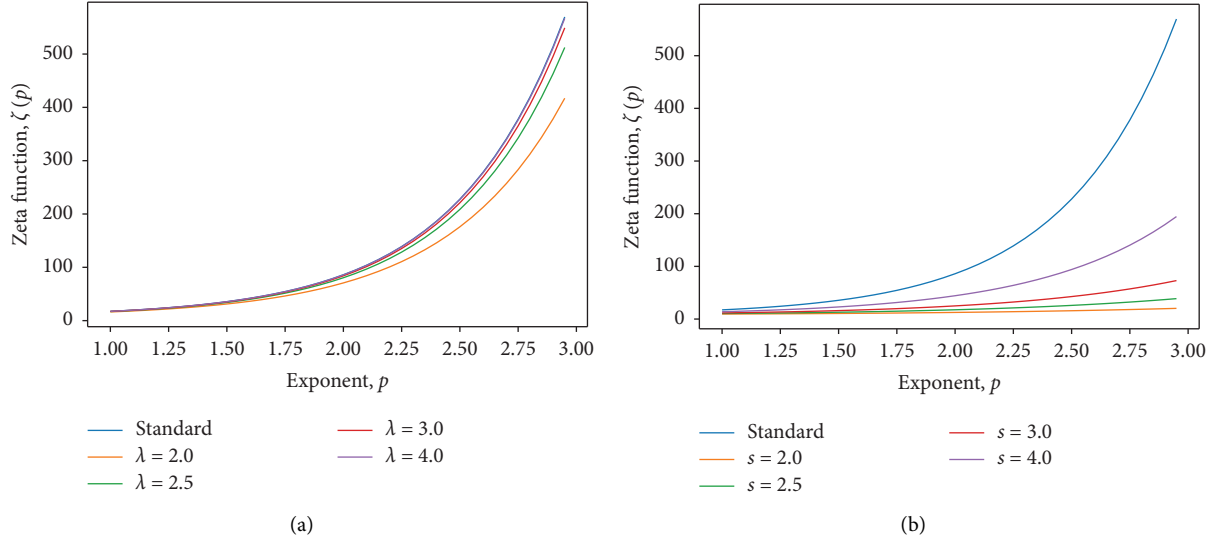


FIGURE 12: Zeta function plotted against the exponent  $p$  for the graph in Figure 7. Subfigure (a) displays the zeta function for the Laplace transform of the graph Laplacian with different values of  $\lambda$  (2, 2.5, 3, and 4). Subfigure (b) illustrates the zeta function for the Mellin transform of the graph Laplacian with various values of  $s$  (2, 2.5, 3, and 4). By increasing  $\lambda$  and  $s$ , we can see that the zeta functions tend to the zeta function of the standard Laplacian (blue curve). This occurs much faster when the Laplace transform is used (a) compared to the Mellin transform (b).

$$\zeta'(p) = \sum_{\lambda_i \neq 0} \{-\ln \lambda_i\} e^{-p \ln \lambda_i}. \quad (34)$$

At the origin, i.e.,  $p = 0$ , we have

$$\zeta'(0) = - \sum_{\lambda_i \neq 0} \ln \lambda_i. \quad (35)$$

The derivative or slope of the zeta function at the origin is another invariant of the heat kernel that can be used for graph characterization [19]. It is simpler than the zeta function because it is parameter independent.

To begin, we analyze the graph depicted in Figure 7 and calculate the derivatives of the zeta function at the origin. The computed values are 1.5686 and  $-3.4012$  for the normalized and unnormalized Laplacian matrices, respectively. Subsequently, we extend our investigation to the generalized versions of both the normalized and unnormalized Laplacian. As illustrated in Figure 13, we observe that in both cases, the values of  $\zeta'(0)$  increase rapidly as the Mellin (or Laplace) exponents,  $s$  (or  $\lambda$ ), increase until constant values of  $\zeta'(0)$  are attained at  $s$  (or  $\lambda$ )  $\approx 9$ . This pattern is a consequence of the diminishing strength of long-range interactions (LRI) as the values of  $s$  (or  $\lambda$ ) increase. Beyond a certain threshold, additional increments in the exponent values result in minimal changes to the LRI, leading to only negligible alterations in the spectrum of the corresponding generalized Laplacian matrix. However, we observe that in the Laplace transform-based case, the value of the derivative of the zeta function at the origin approaches that of standard diffusion more rapidly (see Figures 13(a) and 13(b)) compared to the Mellin transform-based case.

## 5. The Generalized Heat Content

The heat content of a graph represents the total amount of heat retained within the graph over time, with the graph's structure influencing this preservation. The generalized heat content is calculated as the sum of entries in the generalized heat kernel matrix of a graph. For a graph  $G = (V, E)$ , the generalized heat content, denoted by  $Q_t$ , at time,  $t$  is given by

$$Q(t) = \sum_{p \in V} \sum_{q \in V} \mathbf{H}_t(p, q). \quad (36)$$

In particular for hops of length 1 ( $k = 1$ ), equation (36) reduces to the heat content based on the standard Laplacian matrix introduced in [19].

The heat content can be expressed as follows:

$$Q(t) = \sum_{p \in V} \sum_{q \in V} \sum_{i=1}^{|V|} e^{-\lambda_i t} \mathbf{v}_i(p) \mathbf{v}_i(q), \quad (37)$$

where  $\lambda_i$  represents the  $i$ -th eigenvalue of  $\mathbf{H}_t$  and  $\mathbf{v}_i$  the corresponding eigenvectors. Equation (37) captures the total amount of heat in the graph/network at time  $t$ . The heat content  $Q(t)$  can be expanded into a polynomial in time of the form:

$$Q(t) = \sum_{m=0}^{\infty} q_m t^m, \quad (38)$$

where  $q_m$  is given by

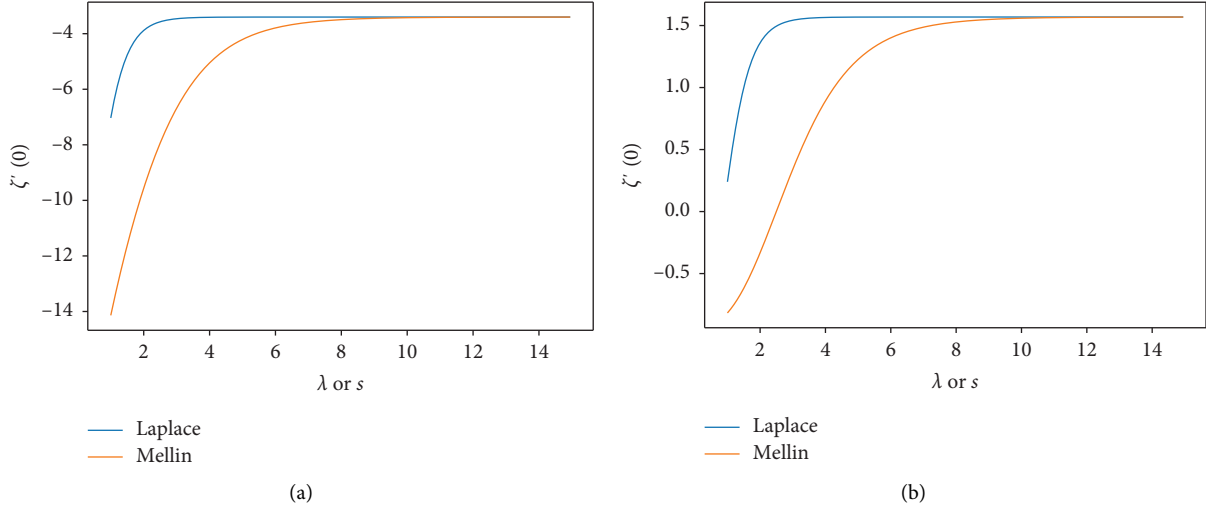


FIGURE 13: Plots illustrating the derivative of the zeta function at the origin for the graph in Figure 7. Panel (a) is for the generalized Laplacian matrix,  $L_G$ . In comparison, the plot in Panel (b) corresponds to the generalized normalized Laplacian (18). Notably, for small values of  $\lambda$  and  $s$ , the Laplace-based case consistently yields higher values than the Mellin-based case. However, as  $\lambda, s \rightarrow \infty$ , the derivatives of the zeta function at the origin converge.

$$q_m = \sum_{i=1}^{|V|} \left\{ \left( \sum_{p \in V} v_i(p) \right)^2 \right\} \frac{(-\lambda_i)^m}{m!}. \quad (39)$$

The coefficients  $q_m$  are uniquely determined by the entries of eigenvectors and eigenvalues, providing a distinctive set of polynomial coefficients for each graph. This uniqueness can serve as a foundation for graph characterization. In the context of graph clustering, feature vectors can be constructed using the  $k$ -leading coefficients, denoted as  $B_k = (q_1, q_2, \dots, q_k)^T$ . This concept will be further explored in subsequent publications.

**5.1. Generalized Heat Content Simulations.** As mentioned earlier, the normalized Laplacian matrix demonstrates superior performance compared to the standard Laplacian in specific scenarios. When it comes to calculating the heat content, we use the normalized Laplacian. This choice is driven by the observation that, in the case of the unnormalized Laplacian, the heat content remains constant over time.

The initial value of the heat content for a given graph at  $t = 0$  is equal to the trace of the identity matrix  $\mathbf{I}$  which is equivalent to the number of vertices,  $|V|$ , in the graph. For the graph illustrated in Figure 7, we have  $Q(0) = 10$ . From Figure 14, it is evident that in the absence of long-range influence (LRI), the heat content decreases rapidly over time (blue dotted curve). Nevertheless, when considering the generalized diffusion based on the Laplacian and Mellin transform, it is apparent that as the values of  $\lambda$  and  $s$  increase, there is a faster drop in the heat content, and the corresponding curves tend to resemble those of the standard diffusion process. The faster decline in heat content observed in the Laplace transform-based case, compared to the Mellin transform-based case, is a result of the stronger influence of long-range interactions (LRI) in the former. Importantly, for

very large graphs, computational complexities associated with heat content calculations can be considerable. To mitigate this challenge, heat content estimation methods leveraging matrix multiplication and random walks can be employed.

**5.2. Heat Content as a Means of Structural Characterization of Graphs with Long-Range Interactions.** We are interested in comparing graphs with scale-free degree distributions to random graphs and finding similarities of the graphs generated by one growing model with different parameters. We will then assess the impact of LRI by using the generalized heat content. With a little algebraic manipulation, the heat content can be written as follows:

$$Q(t) = \sum_{i=1}^{|V|} \alpha_i e^{-\lambda_i t}, \quad (40)$$

where  $\alpha_i = \sum_{p \in V} \sum_{q \in V} v_i(p) v_i(q)$ . This representation views the heat content as a sum of exponential functions with distinct decay rates determined by Laplacian eigenvalues and varying weights ( $\alpha_i$ ) determined by the Laplacian eigenvectors. The asymptotic behavior near zero of the heat content can be described as follows:

$$Q(t)|_{t \rightarrow 0^+} = \sum_i \alpha_i = |V|. \quad (41)$$

For a given initial distribution of heat on a graph, the heat content describes the diffusion of heat with time on the graph. The asymptotic behavior of the heat content has been used in studying the structure of graphs and manifolds [31, 32]. The heat content characterizes the diffusion of heat over time on a graph, starting from a given initial distribution. Researchers have leveraged the asymptotic behavior of the heat content for studying the structural properties of

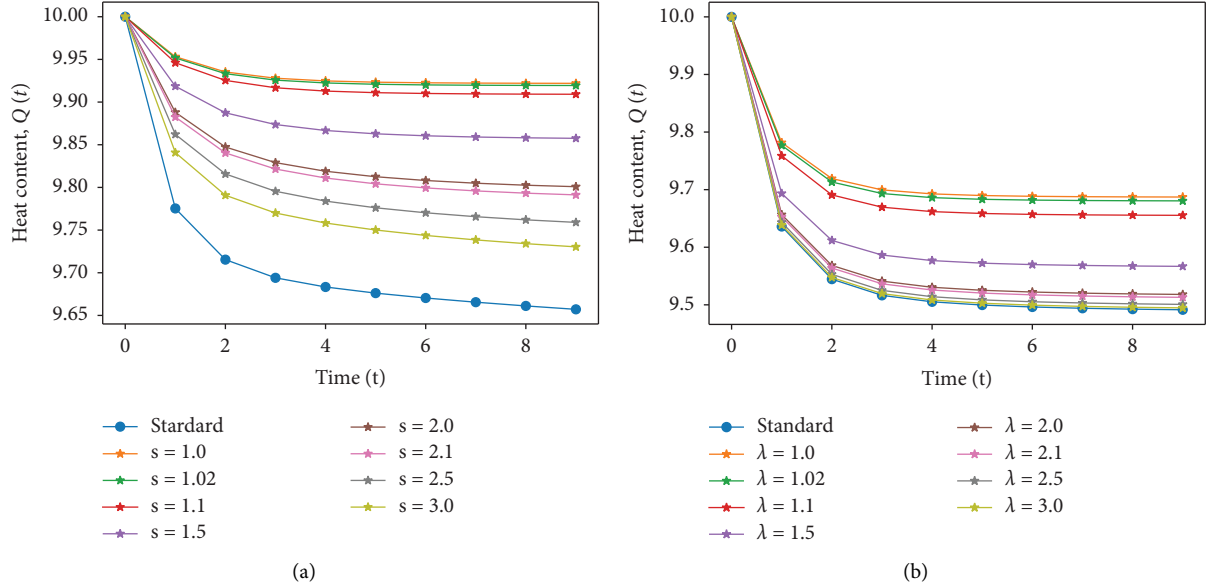


FIGURE 14: Results of simulations for the generalized heat content over time for the graph in Figure 7. Panel (a) depicts the results for various values of the parameter  $s$  in the Mellin transform-based generalized normalized Laplacian matrix, while Panel (b) corresponds to the Laplace transform-based generalized normalized Laplacian for different values of  $\lambda$ . As  $\lambda$  and  $s$  increase, we observe that the heat contents in both panels tend to approach the heat content of the standard Laplacian (depicted by the blue dotted curve) without LRI. Notably, this convergence occurs more rapidly when the Laplace transform is utilized (b) compared to the Mellin transform (a).

graphs and manifolds [31, 32]. The eigenvalues of the normalized Laplacian for a connected undirected graph fall within the range of 0 to 2. Examining equation (40), we observe that the trivial eigenvalue possesses a large corresponding weight,  $\alpha$ , and an exponential decay component that decreases relatively slowly, thereby dominating the heat content curve. To mitigate the dominance of the trivial eigenvalue and to better understand the influence of large eigenvalues, Kang [31] proposed examining the first and second time derivatives of the heat content, given by the following equations:

$$\begin{aligned} \frac{\partial Q}{\partial t} &= - \sum_{i=1}^{|\mathcal{V}|} \alpha_i \lambda_i e^{-\lambda_i t}, \\ \frac{\partial^2 Q}{\partial t^2} &= \sum_{i=1}^{|\mathcal{V}|} \alpha_i \lambda_i^2 e^{-\lambda_i t}. \end{aligned} \quad (42)$$

Smaller eigenvalues are associated with smaller weights, while larger eigenvalues have larger weights. Furthermore, the asymptotic behavior of the first and second derivatives of the heat content can be expressed as follows:

$$\begin{aligned} \left. \frac{\partial Q}{\partial t} \right|_{t \rightarrow 0^+} &= - \sum_i \alpha_i \lambda_i, \\ \left. \frac{\partial^2 Q}{\partial t^2} \right|_{t \rightarrow 0^+} &= \sum_i \alpha_i \lambda_i^2. \end{aligned} \quad (43)$$

Hence, the asymptotic behavior allows for the differentiation of graphs with distinct structures using the initial time derivatives of the heat content. Exploiting this insight,

Kang [31] developed a fast and robust algorithm based on the standard Laplacian to differentiate graphs. He applied this algorithm to compare random graphs generated by the Erdős–Rényi (ER) and the Barabási–Albert (BA) models [1]. In Figure 15, it is evident that the heat content curves for the Barabási–Albert (BA) graphs drop much faster than those of the Erdős–Rényi (ER) graphs. This behavior is attributed to the distinct  $\alpha$  values associated with the Laplacian eigenvalues, excluding the smallest eigenvalue. Intriguingly, in graphs with heavy-tail degree distributions, the asymptotic behavior of the heat content can discern graphs with varying average degrees. This is illustrated in Figure 15(b), where the curves with deep blue colors correspond to graphs with lower average degrees, while the lighter ones correspond to graphs with higher average degrees. In the following paragraph, we will evaluate the influence of long-range interaction (LRI) on the heat content and the derivative of the heat content at the origin in equation (43) when utilizing the generalized Laplacian matrix through the Mellin and Laplace transforms.

We conclude this section by evaluating the impact of long-range influence (LRI) on the heat content (40) and the derivative of the heat content at zero (43) when differentiating random graphs. Figures 16 and 17 depict graphs with nearly identical structures.

Figure 18 illustrates the Laplace-transform-based generalized heat content for various values of  $\lambda$  applied to Barabási–Albert (BA) and Erdős–Rényi (ER) random graphs. As can be seen the long-range interaction has stronger effect in differentiating complex networks having similar structure compared to the case when there is no LRI, and this can be seen a generalization of the results in [31].

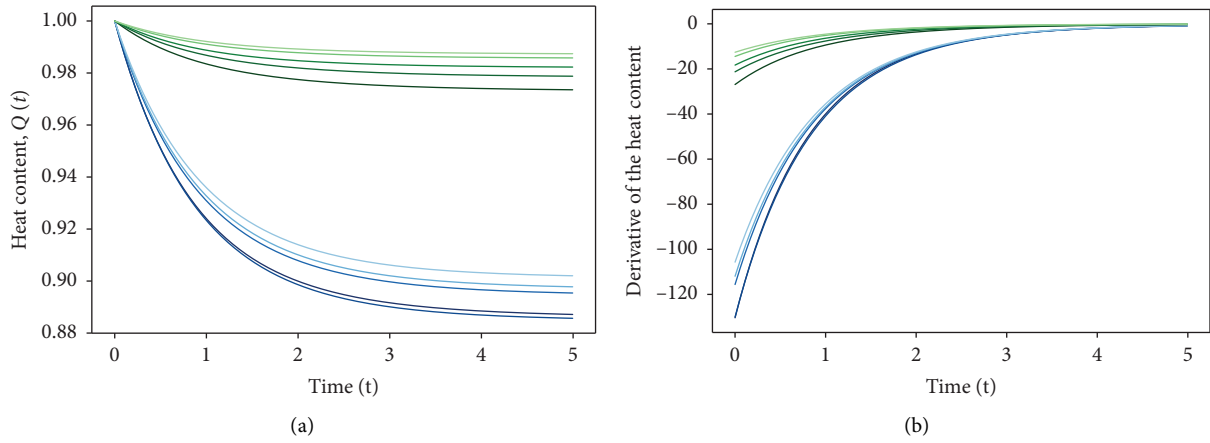


FIGURE 15: Plots of the heat content (using the Laplacian matrix  $L$ ) over time for 5 Barabási-Albert (blue lines) (a) and 5 Erdős-Rényi graphs (green lines), each comprising 1000 nodes with an average degree ranging from 5 to 20. The plot of the first derivative at the origin of the heat content with time is shown in (b). The curves for the first derivative at zero are already distinct compared to the curves of the heat content at the origin, indicating that the first derivative at zero can be useful for characterizing random graphs.

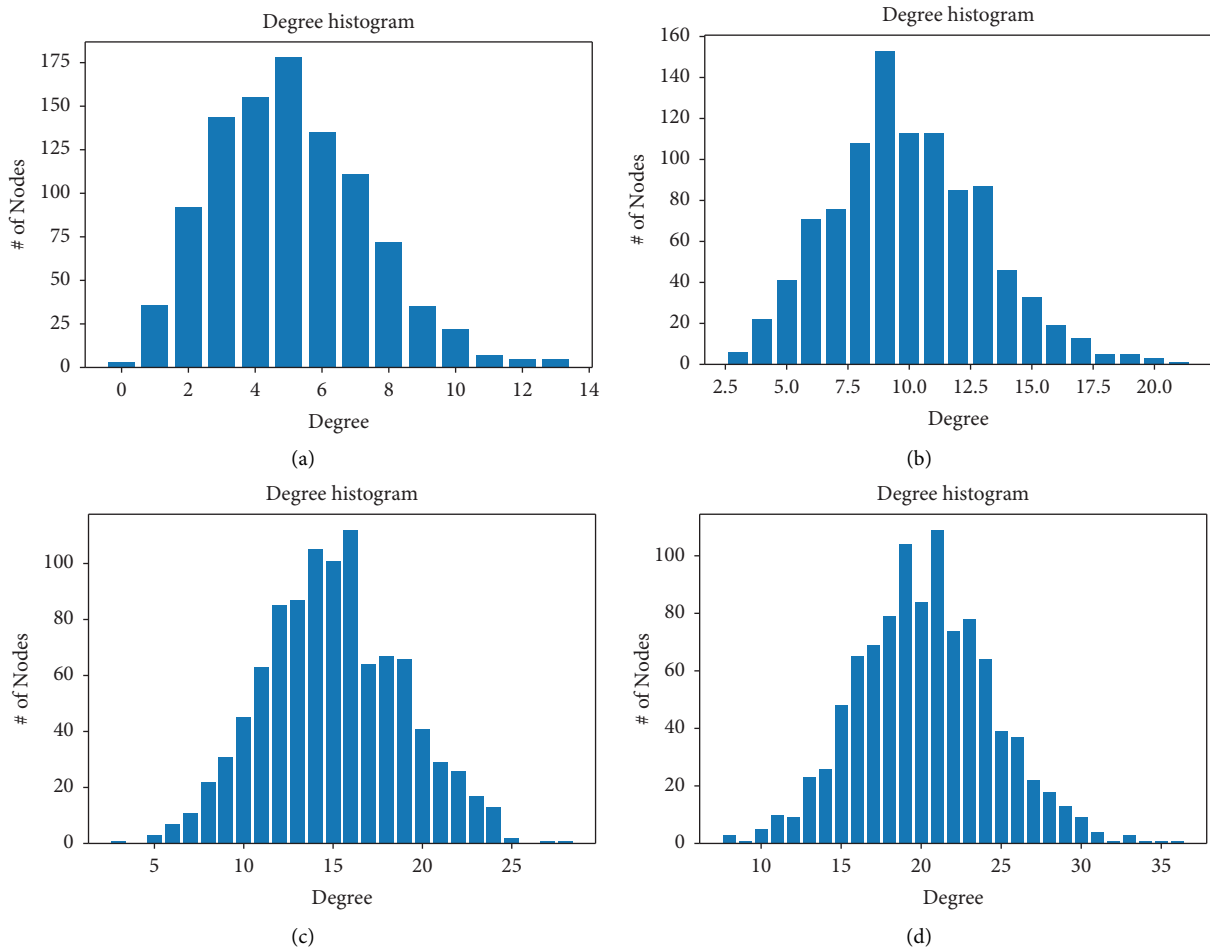


FIGURE 16: Degree distributions of some realizations of ER random graphs having 1000 nodes each with different average degree and whose structure looks very similar. We will show that the derivative of the generalized heat content at the origin is able to distinguish these graphs. (a)  $\langle k \rangle = 5$ . (b)  $\langle k \rangle = 10$ . (c)  $\langle k \rangle = 15$ . (d)  $\langle k \rangle = 20$ .

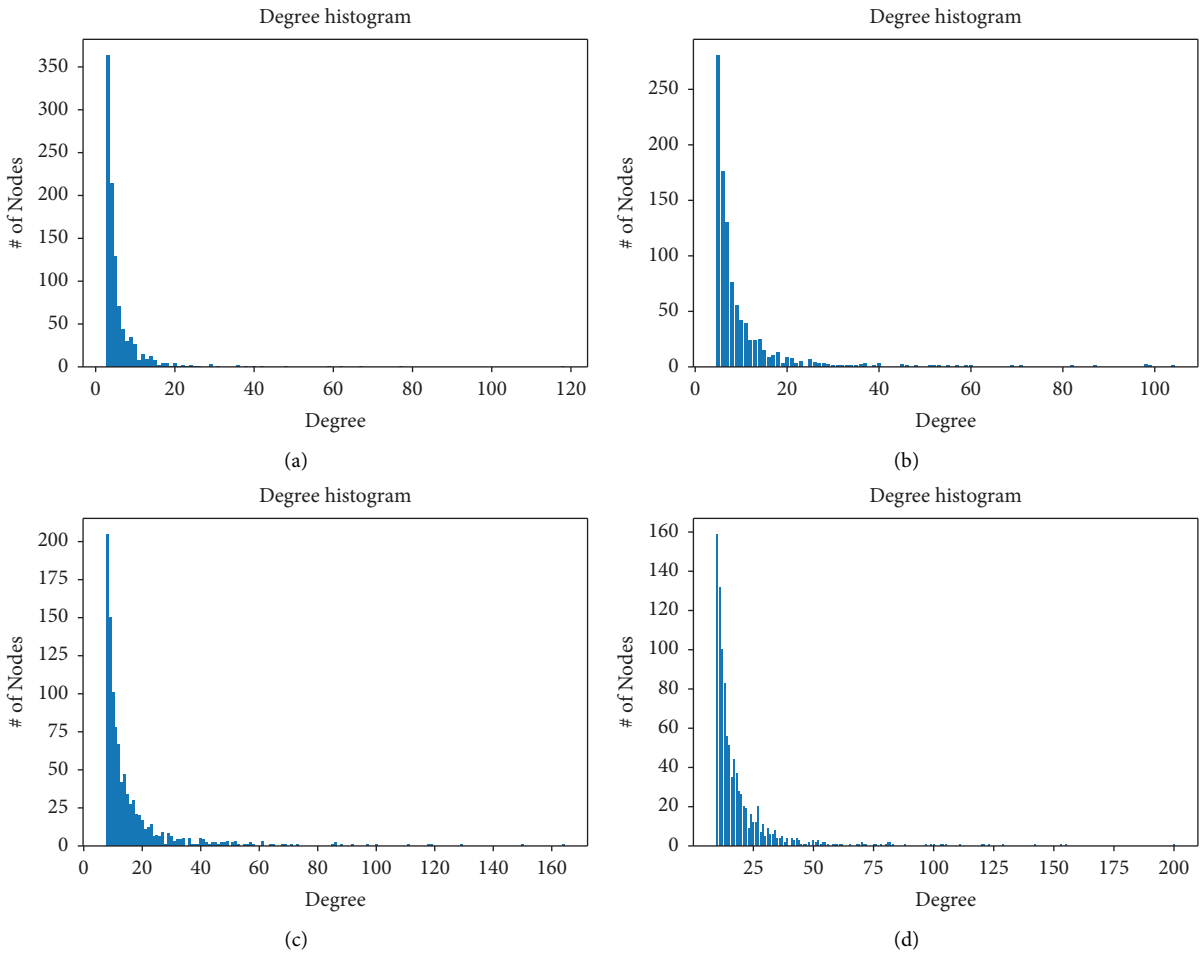


FIGURE 17: Degree distributions of some realizations of Barabási–Albert graphs whose having 1000 nodes with different average degree and whose structure looks very similar. We will show that the derivative of the generalized heat content at the origin is able to distinguish those graphs. (a)  $\langle k \rangle = 5$ . (b)  $\langle k \rangle = 10$ . (c)  $\langle k \rangle = 15$ . (d)  $\langle k \rangle = 20$ .

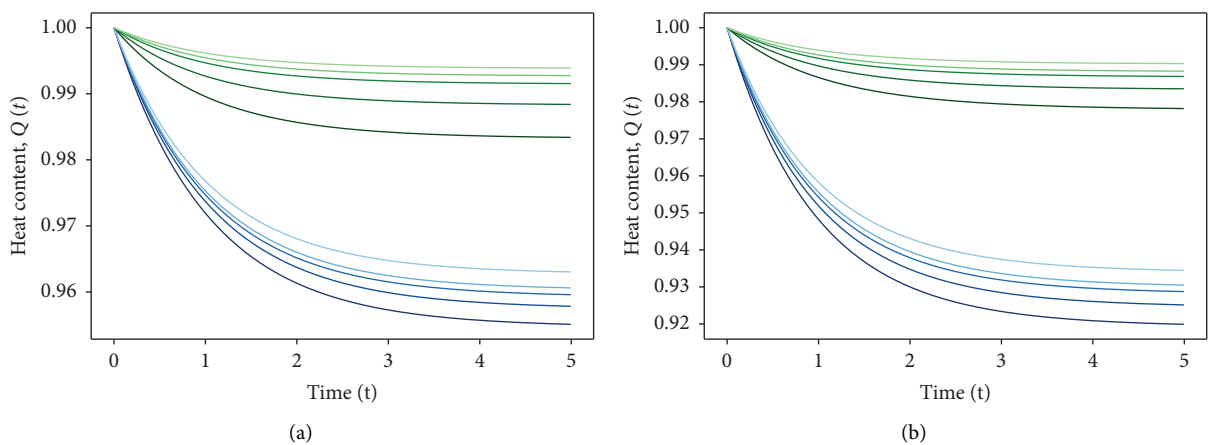


FIGURE 18: Continued.

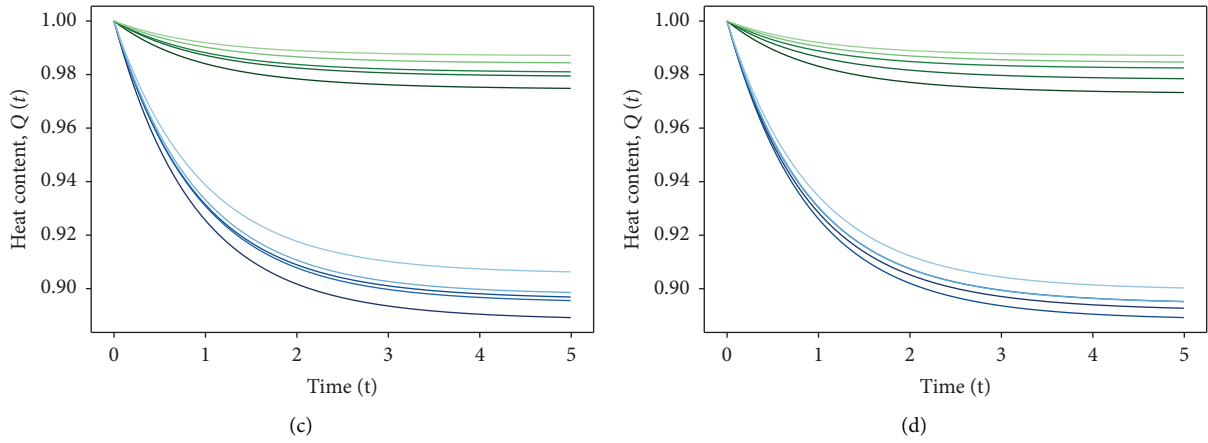


FIGURE 18: The plots in Figure 18 illustrate the behavior of the generalized heat content using the Laplace transform against time for 5 Barabási-Albert (BA) graphs (depicted by blue lines) and 5 Erdős-Rényi (ER) graphs (depicted by green lines). These graphs are constructed with 1000 nodes each, and their average degree falls within the range of 5 to 20. (a)  $\lambda = 1.5$ . (b)  $\lambda = 2$ . (c)  $\lambda = 3$ . (d)  $\lambda = 4$ .

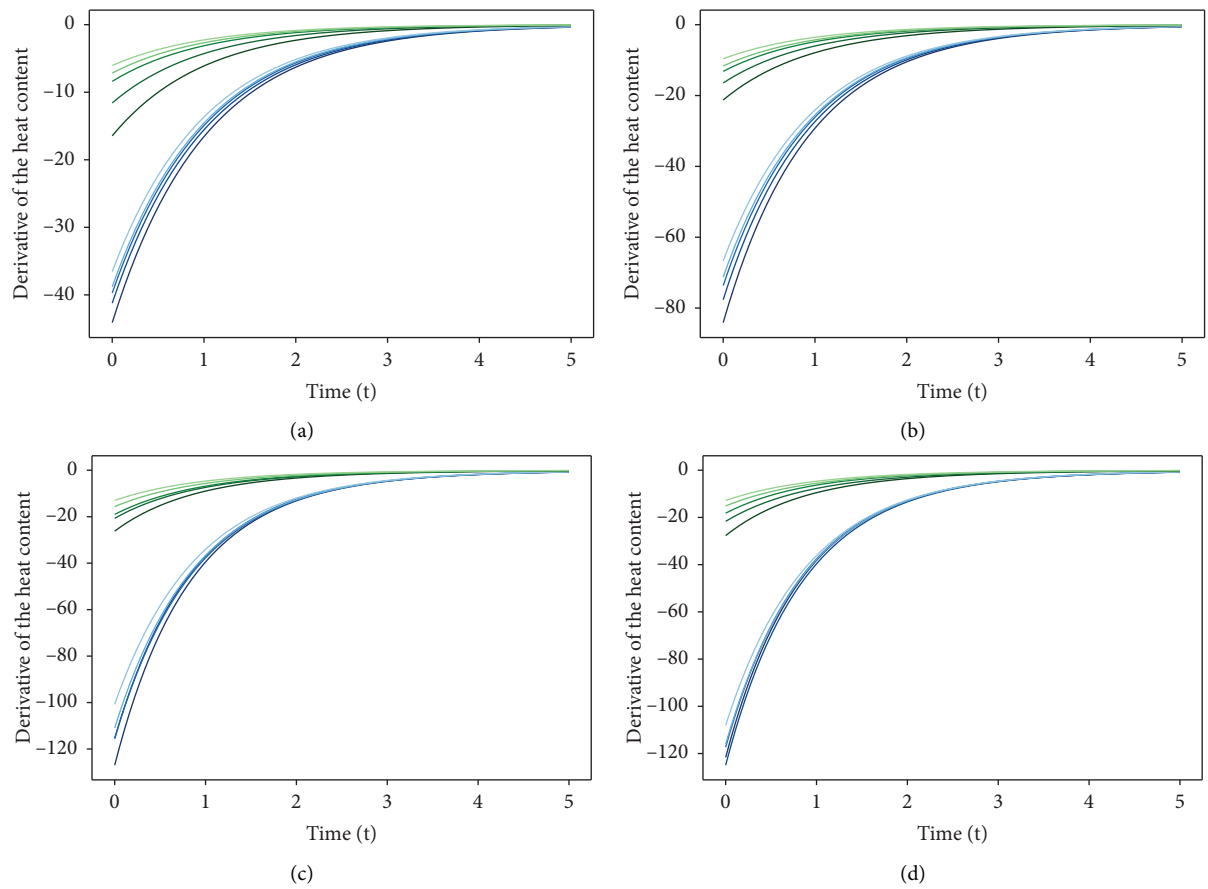


FIGURE 19: Derivative of the generalized heat content at the origin using the Laplace transform against time for 5 Barabási-Albert (BA) graphs (represented by blue lines) and 5 Erdős-Rényi (ER) graphs (depicted by green lines). These graphs consist of 1000 nodes each, with an average degree ranging between 5 and 20. At  $t = 0$ , the curves are distinctly separated, especially for small values of the Laplace exponent ( $\lambda$ ). The introduction of long-range interactions (LRI) further enhances the separation of the curves and contributes to the effective characterization of complex random graphs at  $t = 0$ . (a)  $\lambda = 1.5$ . (b)  $\lambda = 2$ . (c)  $\lambda = 3$ . (d)  $\lambda = 4$ .

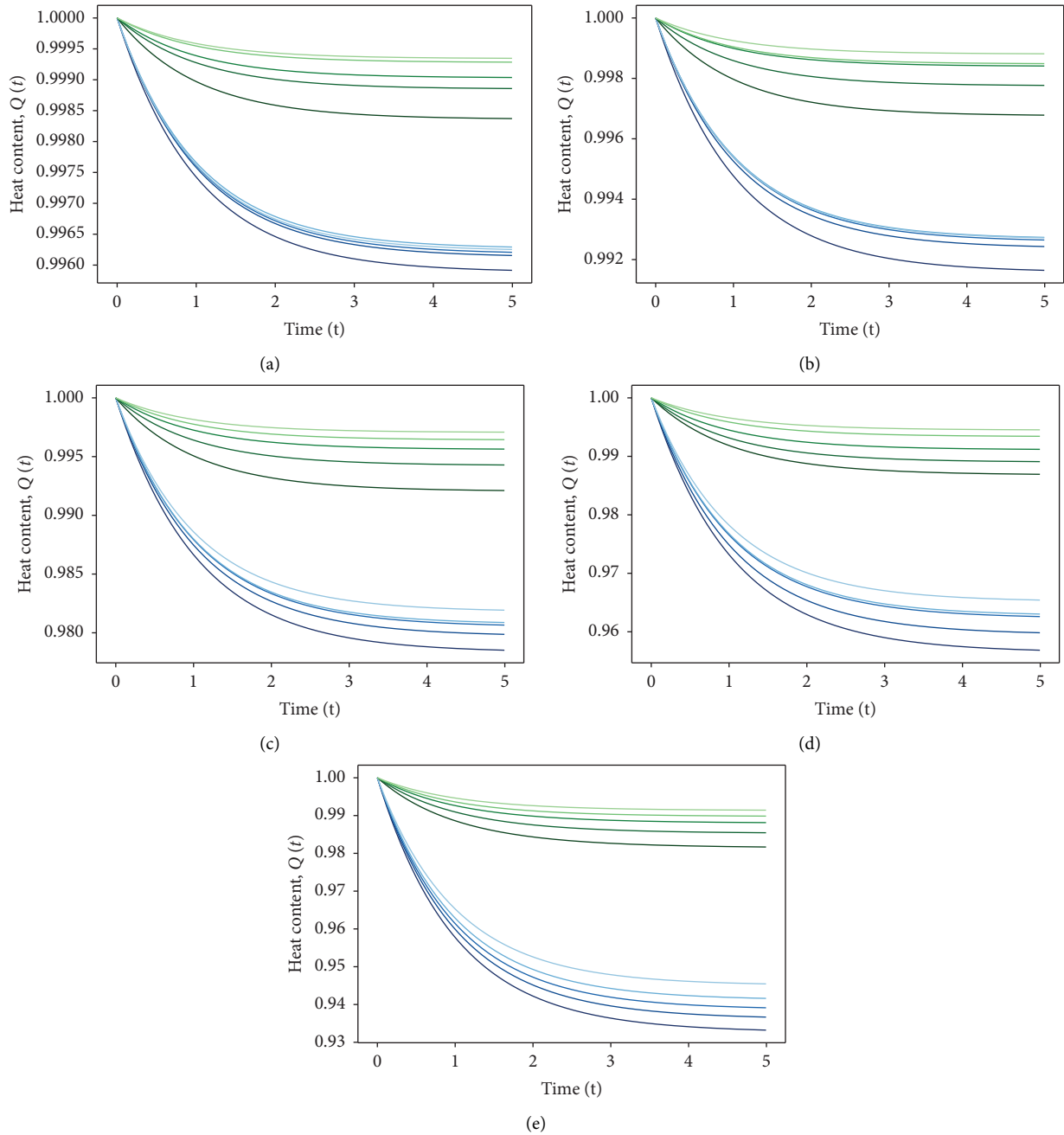


FIGURE 20: Time evolution of the heat content based on the generalized Laplacian matrix using the Mellin transform for 5 Barabási–Albert (BA) graphs (depicted by blue lines) and 5 Erdős–Rényi (ER) graphs (represented by green lines). These graphs consist of 1000 nodes each, with an average degree varying between 5 and 20. As can be seen, the generalized heat content is able to distinguish random graphs having similar structure. The discriminating power increases with value of  $s$  for both BA and ER graphs. (a)  $s = 1.5$ . (b)  $s = 2$ . (c)  $s = 3$ . (d)  $s = 4$ . (e)  $s = 5$ .

For small values of  $\lambda$  and for increasing  $t$  we obtain better curves which are well separated compared to curves in Figure 15(a) when no LRI are considered. On the other hand, as can be seen in Figure 19 the derivative of the heat content at the origin with LRI has the same effect in separating curves at earlier stage ( $t = 0$ ) and the discriminating power is much greater for small values of  $\lambda$ . Similar results are obtained when using the Mellin transform as shown in Figures 20 and 21.

## 6. On Computation of the Generalized Heat Kernel and Limitations

The results obtained in this paper demonstrate that the generalized heat kernel can obtain better graph characterization compared to the standard heat kernel (without long-range interactions). However, computing all the  $k$ -path Laplacian matrices  $L_k$  ( $1 \leq k \leq d_{\max}$ ) can be costly for large networks. To generate the distance matrix, it is necessary to

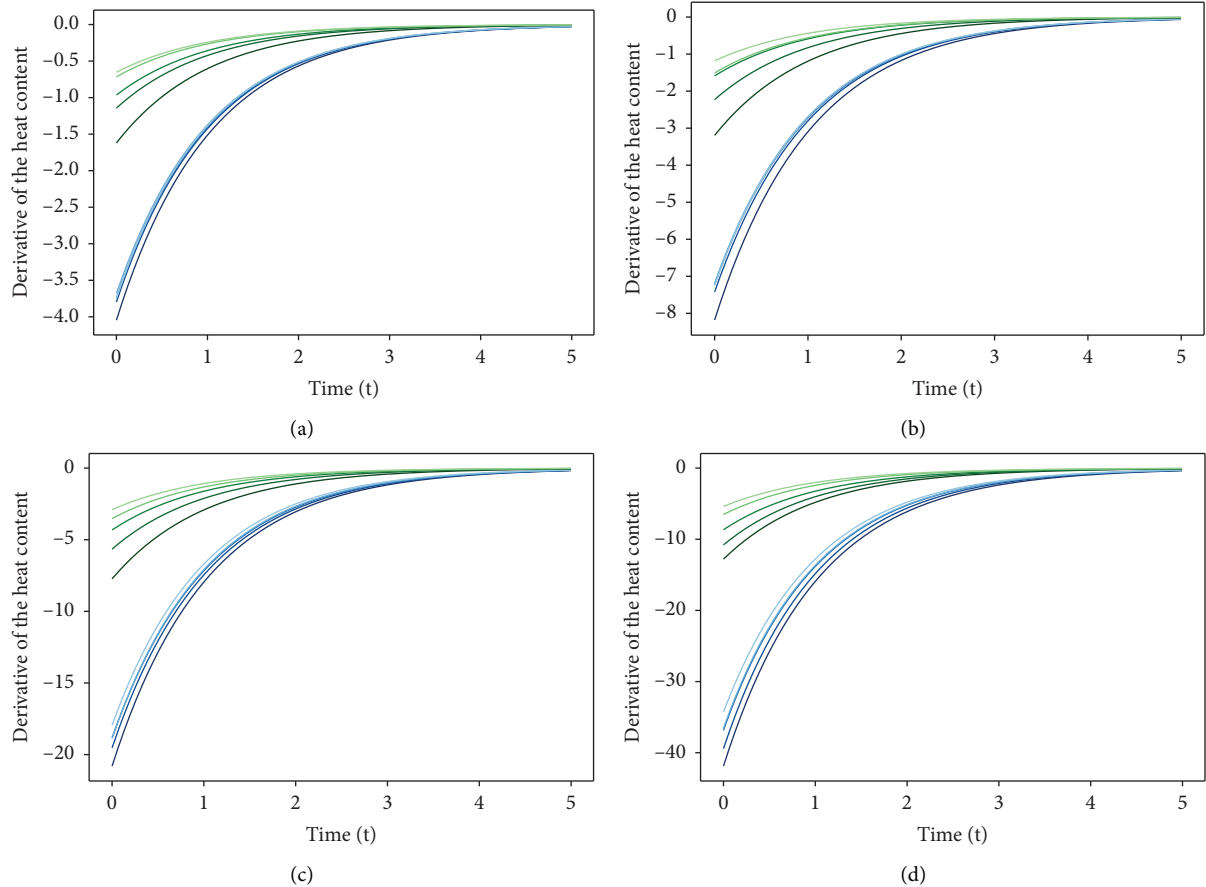


FIGURE 21: Time-dependent behavior of the derivative of the heat content at  $t = 0$  for Barabási-Albert (BA) graphs (represented by blue lines) and 5 Erdős-Rényi (ER) graphs (depicted by green lines). Each graph consists of 1000 nodes with an average degree ranging from 5 to 20. The derivative is computed based on the generalized Laplacian matrix using the Mellin transform. (a)  $s = 1$ . (b)  $s = 2$ . (c)  $s = 3$ . (d)  $s = 4$ .

identify all pairs of nodes at distance  $k$  and solve the all-pairs shortest-paths problem (APSP). The shortest path problem is encountered in various facets of complex network analysis, including the investigation of distance-based centrality measures, average path length, and the small-world phenomenon, among other applications. All these approaches, including those involving path Laplacian that contribute to the development of the generalized heat kernel, will benefit from the ongoing development of new methods for solving the All-Pairs Shortest Paths (APSP) problem [33]. For the same considerations discussed in [9], we avoid computing all  $k$ -path Laplacian. If, for instance, there is indication that a particular signal does not extend beyond the second nearest neighbors, it suffices to compute  $L_1$  and  $L_2$ , leading to a reduction in computation cost.

## 7. Conclusions and Future Outlook

We introduced the concept of the generalized heat kernel for graphs and networks, representing a natural extension of the standard heat kernel. This kernel serves as the fundamental solution to the generalized diffusion equation, capturing the flow process where substances or information propagate not only through direct interactions but also via long-range

interactions (LRI). The incorporation of LRI is achieved through the Mellin and Laplace transforms applied to the  $k$ -path Laplacian matrices, as proposed by Estrada [9]. Expanding upon the work in [19], we investigated the applicability of generalized heat kernel invariants for graph characterization. These invariants encompass the heat kernel trace, zeta function, derivative of the zeta function at the origin, and heat content. Our results indicate that these invariants exhibit superior performance in distinguishing graphs compared to standard heat kernel methods. Future extensions of this work include practical applications, particularly in object clustering using graphs derived from objects. In addition, exploring the geometry of graphs residing on manifolds is a promising avenue. This involves embedding graph nodes into points in a vector space on a manifold [34], enabling the extension of generalized heat kernel invariants to features with direct geometric interpretations, such as Euler characteristic, torsion of the mean, and Gaussian curvature. Another direction for future exploration is the development of faster computational methods for the generalized heat kernel, drawing inspiration from ideas proposed in [35]. In closing, we anticipate that the generalized heat kernel will become a valuable addition to the extensive array of graph-theoretic and algebraic tools

employed across various scientific disciplines. The study of the mathematical properties of the generalized heat kernel opens up a novel path in the field of algebraic graph theory.

## Data Availability

The data used to support the findings of this study were simulated on a computer or manufactured by ourselves. The code is available on request.

## Conflicts of Interest

The authors declare that they have no conflicts of interest.

## Acknowledgments

Franck Kalala Mutombo would like to thank Robert Bosch Stiftung and AIMS-South Africa for providing a research grant and support during his stay at AIMS Research Center. Alice Nyanzi would like to thank the National Research Foundation (NRF) for funding her studies at AIMS and the University of Stellenbosch. Alice would also like to thank Stellenbosch University for publishing her master's thesis on SUNScholar Research Repository at <https://scholar.sun.ac.za/handle/10019.1/105064>. Simukai W. Utete expresses gratitude for the support received from the National Research Foundation (NRF), South Africa, while being a member of the AIMS Research Centre.

## References

- [1] E. Estrada, *The Structure of Complex Networks: Theory and Applications*, OUP Oxford, Oxford, UK, 2011.
- [2] M. E. J. Newman, "Scientific collaboration networks. II. shortest paths, weighted networks, and centrality," *Physical Review E-Statistical Physics, Plasmas, Fluids, and Related Interdisciplinary Topics*, vol. 64, no. 1, Article ID 016132, 2001.
- [3] M. E. J. Newman, "The structure and function of complex networks," *SIAM Review*, vol. 45, no. 2, pp. 167–256, 2003.
- [4] M. E. J. Newman, *Networks: An Introduction*, OUP Oxford, Oxford, UK, 2010.
- [5] S. Barbarossa and M. Tsitsvero, "An introduction to hypergraph signal processing," in *2016 IEEE International Conference on Acoustics, Speech and Signal Processing (ICASSP)*, pp. 6425–6429, Shanghai, China, March 2016.
- [6] A. Aleta and Y. Moreno, "Multilayer networks in a nutshell," *Annual Review of Condensed Matter Physics*, vol. 10, no. 1, pp. 45–62, 2019.
- [7] M. Kivelä, A. Arenas, M. Barthélemy, J. P. Gleeson, Y. Moreno, and M. A. Porter, "Multilayer networks," *Journal of Complex Networks*, vol. 2, no. 3, pp. 203–271, 07 2014.
- [8] P. Holme and J. Saramäki, "Temporal networks," *Physics Reports*, vol. 519, no. 3, pp. 97–125, 2012.
- [9] E. Estrada, "Path Laplacian matrices: introduction and application to the analysis of consensus in networks," *Linear Algebra and Its Applications*, vol. 436, no. 9, pp. 3373–3391, 2012.
- [10] F. Chazal and B. Michel, "An introduction to topological data analysis: fundamental and practical aspects for data scientists," 2017, <https://arxiv.org/abs/1710.04019>.
- [11] V. Salnikov, D. Cassese, and R. Lambiotte, "Simplicial complexes and complex systems," *European Journal of Physics*, vol. 40, no. 1, Article ID 014001, 2018.
- [12] R. Kondor and J.-P. Vert, *Diffusion Kernels, Kernel Methods in Computational Biology*, MIT Press, Cambridge, MA, USA, 2004.
- [13] D. López-Pintado, "Diffusion in complex social networks," *Games and Economic Behavior*, vol. 62, no. 2, pp. 573–590, 2008.
- [14] E. Estrada, F. Kalala-Mutombo, and A. Valverde-Colmeiro, "Epidemic spreading in networks with nonrandom long-range interactions," *Physical Review E*, vol. 84, no. 3, Article ID 036110, 2011.
- [15] E. Estrada, E. Hameed, N. Hatano, and M. Langer, "Path Laplacian operators and super diffusive processes on graphs i. one-dimensional case," *Linear Algebra and Its Applications*, vol. 523, pp. 307–334, 2017.
- [16] E. Estrada, L. V. Gambuzza, and M. Frasca, "Long-range interactions and network synchronization," *SIAM Journal on Applied Dynamical Systems*, vol. 17, no. 1, pp. 672–693, 2018.
- [17] H. Ma, H. Yang, M. R. Lyu, and I. King, "Mining social networks using heat diffusion processes for marketing candidates selection," in *Proceedings of the 17th ACM conference on Information and knowledge management*, pp. 233–242, Napa Valley, CA, USA, October 2008.
- [18] R. Kasprzak, "Diffusion in networks," *Journal of Telecommunications and Information Technology*, vol. 2, pp. 99–106, 2012.
- [19] B. Xiao, E. R. Hancock, and R. C. Wilson, "Graph characteristics from the heat kernel trace," *Pattern Recognition*, vol. 42, no. 11, pp. 2589–2606, 2009.
- [20] J. M. Kleinberg, "Navigation in a small world," *Nature*, vol. 406, no. 6798, p. 845, 2000.
- [21] F. Chung, "The heat kernel as the page rank of a graph," *Proceedings of the National Academy of Sciences*, vol. 104, no. 50, pp. 19735–19740, 2007.
- [22] G. Chinta, J. Jorgenson, and A. Karlsson, "Heat kernels on regular graphs and generalized Ihara zeta function formulas," *Monthly Magazines For Mathematics*, vol. 178, no. 2, pp. 171–190, 2015.
- [23] T. Martin, *Barlow, Random Walks and Heat Kernels on Graphs*, vol. 438, Cambridge University Press, Cambridge, UK, 2017.
- [24] E. Merkurjev, A. L. Bertozzi, and F. Chung, "A semi-supervised heat kernel page rank MBO algorithm for data classification," *Communications in Mathematical Sciences*, vol. 16, no. 5, pp. 1241–1265, 2018.
- [25] F. Chung and O. Simpson, "Computing heat kernel page rank and a local clustering algorithm," *European Journal of Combinatorics*, vol. 68, pp. 96–119, 2018.
- [26] R. K. C. Fan, *Spectral Graph Theory, Number 92*, American Mathematical Society, Providence, RI, USA, 1997.
- [27] S. Butler and J. Grout, "A construction of co-spectral graphs for the normalized Laplacian," *Electronic Journal of Combinatorics*, vol. 18, no. 1, p. 8, 2011.
- [28] A. Daniel, "Schult, Exploring network structure, dynamics, and function using NetworkX," in *Proceedings of the 7th Python in Science Conference SciPy*, pp. 11–15, Pasadena, CA, USA, August 2008.
- [29] O. Knill, "The zeta function for circular graphs," 2013, <https://arxiv.org/abs/1312.4239>.

- [30] F. Friedli and A. Karlsson, “Spectral zeta functions of graphs and the Riemann zeta function in the critical strip,” *Tohoku Mathematical Journal*, vol. 69, no. 4, pp. 585–610, 2017.
- [31] J. Kang, *Image Processing and Understanding Based on Graph Similarity Testing: Algorithm Design and Software Development*, University of Massachusetts, Amherst, MA, USA, 2017.
- [32] M. Vandenberg and P. Gilkey, “Heat content asymptotics of a riemannian manifold with boundary,” *Journal of Functional Analysis*, vol. 120, no. 1, pp. 48–71, 1994.
- [33] A. Gubichev, S. Bedathur, S. Seufert, and G. Weikum, “Fast and accurate estimation of shortest paths in large graphs,” in *Proceedings of the 19th ACM International Conference on Information and Knowledge Management*, pp. 499–508, Toronto, Canada, October 2010.
- [34] H. ElGhawalby and E. R. Hancock, “Heat kernel embeddings, differential geometry and graph structure,” *Axioms*, vol. 4, no. 3, pp. 275–293, 2015.
- [35] Y. Lin and Y. Wu, “On-diagonal lower estimate of heat kernels on graphs,” *Journal of Mathematical Analysis and Applications*, vol. 456, no. 2, pp. 1040–1048, 2017.